

Learning-Based Algorithms for Vessel Tracking: A Review

Dengqiang Jia^a, Xiahai Zhuang^{b,*}

^a*School of Naval Architecture, Ocean and Civil Engineering, Shanghai Jiao Tong University, Shanghai, China*

^b*School of Data Science, Fudan University, Shanghai, China*

Abstract

Developing efficient vessel-tracking algorithms is crucial for imaging-based diagnosis and treatment of vascular diseases. Vessel tracking aims to solve recognition problems such as key (seed) point detection, centerline extraction, and vascular segmentation. Extensive image-processing techniques have been developed to overcome the problems of vessel tracking that are mainly attributed to the complex morphologies of vessels and image characteristics of angiography. This paper presents a literature review on vessel-tracking methods, focusing on machine-learning-based methods. First, the conventional machine-learning-based algorithms are reviewed, and then, a general survey of deep-learning-based frameworks is provided. On the basis of the reviewed methods, the evaluation issues are introduced. The paper is concluded with discussions about the remaining exigencies and future research.

Keywords: Vessel tracking, Learning-based algorithms, Review

1. Introduction

Blood vessels, spread throughout the human body, constitute a significant part of the circulatory system. All body tissues rely on the normal functioning of different vessels such as cerebral arteries, retinal vessels, carotid arteries, pulmonary arteries, and coronaries. Any abnormal change in or damage to the vessels will be manifested as diseases at different levels (e.g., stroke, arteriosclerosis, cardiovascular diseases, and hypertension). Medical imaging and image analysis enable novel technologies and applications for better diagnosis and treatment of blood-vessel diseases. Tracking the target vessels from the wide field of view of medical images is a prerequisite for the localization and identification of abnormal vessels or regions of interest. However, manual annotation, which usually demands expertise, is particularly time-consuming and tedious.

Vessel tracking aims to solve the problems encountered in vessel image analysis, including key-point (seed point) detection, centerline extraction, and vascular segmentation. These problems considerably differ because of the wide array of vessel anatomies and image characteristics. Accordingly, the problematic factors are categorized into two groups: those related to vessel morphologies (e.g., small size, branching pattern, tortuosity, and severe stenosis of vessels) and image characteristics (e.g., low contrast, noise, artifacts, dislocation, and adjacent hyper-intense structures).

Localizing the key points and recognizing the key patterns of vascular structures are fundamental to perform vessel tracking; building models based on various assumptions on vascular appearances (i.e., the prior knowledge and intrinsic features) is also important. Exploring such problems facilitates the devel-

opment of new algorithms, particularly in learning-based tracking methods.

In the literature, several articles focus on the survey of vessel-tracking methods. To the best of our knowledge, [Suri et al. \(2002\)](#) published the first survey on this topic. They concentrated on skeleton and indirect techniques for vascular segmentation. In addition to vessel-tracking methods, [Kirbas and Francis \(2004\)](#) particularly reviewed the methods of detecting similar vessel characteristics, such as neurovascular and tubular structures. The review of [Lesage et al. \(2009\)](#) further focused on lumen segmentations. They categorized the methodologies according to three aspects (i.e., models, features, and extraction schemes) and provided general considerations for each aspects.

Recently, more survey papers for tracking the vessels of certain organs in specific imaging modality, e.g., cerebral vessel segmentation from magnetic resonance (MR) images ([Klepaczko et al., 2016](#)), coronary reconstruction from X-ray angiography ([Çimen et al., 2016](#)), and lung vessel detection from computed tomography angiography (CT) ([Rudyanto et al., 2014](#)), have been published. Reviews on retinal vessel segmentation were presented in the work ([Abramoff et al., 2010](#); [Fraz et al., 2012b](#); [Khan et al., 2019](#); [L Srinidhi et al., 2017](#); [Mansour, 2017](#); [Pohankar and Wankhade, 2016](#); [Singh and Kaur, 2015](#); [Soomro et al., 2019](#); [Vostatek et al., 2017](#)). Particularly, [Moreno and Smedby \(2015\)](#) were interested in formulating general methods for enhancement technologies, and [Kerrien et al. \(2017\)](#) focused on modeling approaches. In view of the potential of learning-based methods for tracking retinal vessels, [Moccia et al. \(2018\)](#) and [Zhao et al. \(2019\)](#) reviewed the principles and applications. [Soomro et al. \(2019\)](#) particularly focused on deep-learning-based works of retinal blood vessel segmentation.

1.1. Aims of this paper

This work aims to provide an up-to-date review of vessel tracking based on machine-learning-methods, also referred to

*Corresponding author

Email address: zzh@fudan.edu.cn (Xiahai Zhuang)

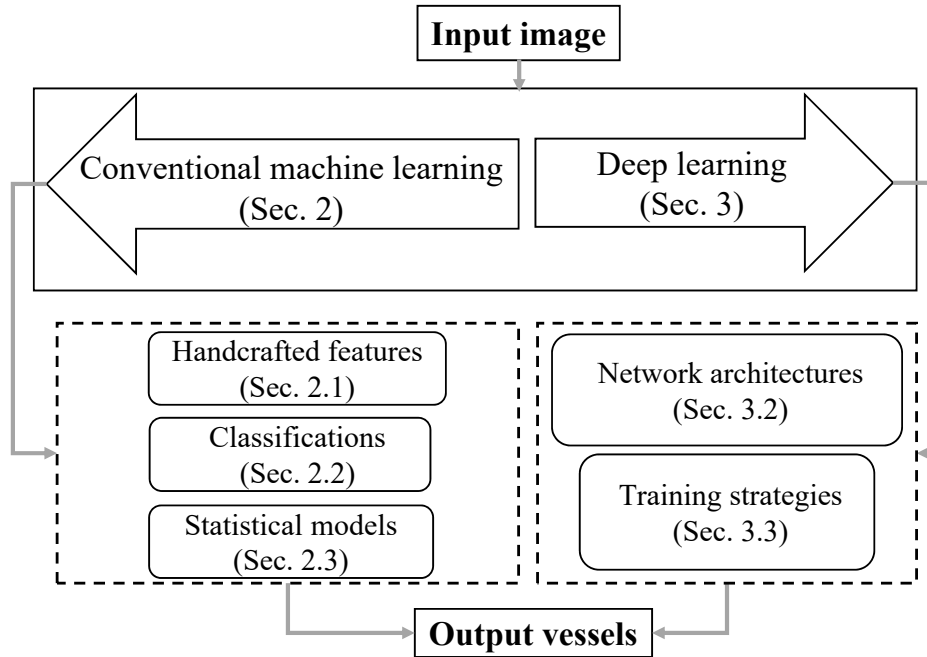


Fig. 1. Recapitulative diagram of vessel tracking using learning-based methods.

as learning-based methods. We focus on the learning-based methods for tracking vessels of various organs using different imaging modalities. The recapitulative diagram of the learning-based methods for vessel tracking is shown in Fig. 1. To cover the articles to a feasible extent, a search for the term vessel/vascular segmentation/extraction has been performed using engines such as PubMed ¹, IEEE Xplore ², and Google Scholar ³. Among over 300 collated articles, the focus of attention was on papers published during the last 10 years. Note that this article does not cover all the details of databases and evaluation standards that can be found in the literature (Hameeteman et al., 2011; Kirisli et al., 2013; Moccia et al., 2018; Rudyanto et al., 2014; Schaap et al., 2009; Vostatek et al., 2017; Yan et al., 2018).

The rest of the paper is organized as follows. Section 2 reviews the vessel tracking methods using conventional machine learning. Section 3 reviews the vessel tracking approaches using deep learning. Based on the reviewed methods, Section 4 introduces the evaluation issues. Finally, Section 5 concludes the review and explores potential directions for future work on learning-based methods for vessel tracking.

2. Vessel tracking using conventional machine learning

This section reviews the vessel-tracking works that employ conventional learning-based algorithms including the methodologies of hand-crafted features, classifications and statistical models. Tables 1-3 summarize the decomposition of a selection of representative works in this field according to the applications. Tables 4 summarizes the existing conventional machine-

learning-based works by grouping them into different subcategories.

2.1. Hand-crafted features

A broad definition of hand-crafted features is provided in (Lesage et al., 2009). Conventional machine-learning-based methods train models with numerous hand-crafted features, which should be well-designed according to the applications. These features (i.e., global and local features) can be obtained by a series of filters such as those given in (Agam et al., 2005; Frangi et al., 1998; Manniesing et al., 2006). Vukadinovic et al. (2010) used a set of features for classifying the calcium candidate object of blood vessels. These features include smoothed intensity, Gaussian derivative features, and a set of shape features including spatial locations (distance to the lumen). Bogunović et al. (2012) extracted a set of labeled bifurcation feature vectors of vessels to train the classifier. Mehmet et al. (2016) extracted local features based on image intensity, intensity gradient, sample positions, and angles. They claimed that the Hessian-matrix-based features can aid in distinguishing between tubular and non-tubular structures.

One application of hand-crafted features is in the development of learning-based kernels. Poletti and Grisan (2014) learned a set of optimal discriminative convolution kernels to be used in AdaBoost classifications. The multi-kernel learning method proposed in (Liu et al., 2014) utilizes the features from the Hessian-matrix-based vesselness measures, multi-scale Gabor filter responses, and multi-scale line strengths. Lesage et al. (2016) learned the non-parametric kernel with likelihood terms of direction and radius transition priors. To estimate the vessel direction and diameter, Asl et al. (2017) formulated a kernelized covariance matrix from the training data.

¹<http://www.ncbi.nlm.nih.gov/pubmed>

²<http://ieeexplore.ieee.org>

³<http://scholar.google.com>

Table 1 Overview of conventional machine-learning-based methods for tracking **retinal vessels**: the evaluation metrics and datasets are presented in Section 4; see list of abbreviations at the bottom.

Authors	Methods	Data	Experiment	Results
Becker et al. (2013)	Boosting-based, learning kernels	Retinal colored image, DRIVE	20 for training, 20 for testing, one-off train + test	Precision-recall curves
Sironi et al. (2015)	Learning separable filters	Retinal colored image, DRIVE	20 for training, 20 for testing, one-off train + test	AUC=0.962
Annunziata and Trucco (2016)	Convolutional sparse coding-filler learning	Retinal colored image, DRIVE Retinal colored image, STARE	20 for training, 20 for testing, one-off train + test 19 for training, 1 for testing, leave-one-out	AUPRC=0.87 AUPRC=0.86
Gu et al. (2017)	Boosting-based, structured features	Retinal colored image, DRIVE Retinal colored image, STARE Retinal colored image, CHASE-DB1 Retinal colored image, HRF	20 for training, 20 for testing, one-off train + test 20 images, five-fold cross-validation 14 for training, 14 for testing, one-off train + test half for training, half for testing, one-off train + test	Pr=0.7931, Re=0.7595, Sp=0.9711 Pr=0.7761, Re=0.7791, Sp=0.9741 Pr=0.6660, Re=0.6850, Sp=0.9664 Pr=0.7775, Re=0.7602, Sp=0.9795
Javidi et al. (2017)	Dictionary learning, vessel and non-vessel features	Retinal colored image, DRIVE	20 for training, 20 for testing, one-off train + test	Acc=0.9446
Kalata and Gooya (2017)	Hierarchical probabilistic framework, intensity features of the cross sections	Retinal colored image, REVIEW Retinal colored image, DRIVE	16 images, leave-one-out 40 images, leave-one-out	Acc=0.9446 Acc=0.970
Orlando et al. (2017)	SVM, features in CRF	Retinal colored image, DRIVE Retinal colored image, STARE Retinal colored image, CHASE-DB1 Retinal colored image, HRF	20 for training, 20 for testing, one-off train + test 19 for training, 1 for testing, leave-one-out 8 for training, 20 for testing, one-off train + test 5 for training, 40 for testing, one-off train + test	Pr=0.7854, Se=0.7897, Sp=0.9684 Pr=0.7740, Se=0.7680, Sp=0.9738 Pr=0.7438, Se=0.7277, Sp=0.9712 Pr=0.6950, Se=0.7794, Sp=0.9650
Zhang et al. (2017a)	Random forest, gaussian-based filters wavelet transform	Retinal colored image, DRIVE Retinal colored image, STARE Retinal colored image, CHASE-DB1	20 for training, 20 for testing, one-off train + test 19 for training, 1 for testing, leave-one-out 27 for training, 1 for testing, leave-one-out	Acc=0.9466, AUC=0.9703, Se=0.7861, Sp=0.9712 Acc=0.9547, AUC=0.9740, Se=0.7882, Sp=0.9729 Acc=0.9502, AUC=0.9706, Se=0.7644, Sp=0.9716

* List of abbreviations: Acc=accuracy; AUC=area under the ROC curve; AUPRC=area under the precision-recall curve; CRF=conditional random field; Pr=precision; Re=recall; REVIEW (Al-Diri et al., 2008); Se=sensitivity; Sp=specificity; SVM= support vector machine.

Table 2

Overview of conventional machine-learning-based methods for tracking **coronary vessels**: the evaluation metrics and datasets are presented in Section 4; see list of abbreviations at the bottom.

Authors	Methods	Data	Experiment	Results
Schaap et al. (2011)	Nonlinear regression, point-distribution and intensity model	Coronary CTA, local data Coronary CTA, CAT08	82 for training, 1 for testing, leave-one-out 8 for training, 24 for testing, one-off train + test	Distance=0.15mm AI=0.23mm, OF=0.725, OT=0.971, OV=0.969
Lesage et al. (2016)	Bayesian vessel model and particle-filtering, flux-based image feature	Coronary CTA, local data	10 for training, 51 for testing	AI=0.25mm, OT=0.925, OV=0.862
Mehmet et al. (2016)	Boosting-based, image features, orientation and scale	Coronary CTA, local data	90 for training, 20 for testing	Se > 0.9, Sp > 0.9

* List of abbreviations: AI=average inside; CTA = computed tomography angiography; OF=overlap until first error; OT=overlap with the clinically relevant part of the vessel; OV=overlap; Se=sensitivity; Sp=specificity.

Table 3

Overview of conventional machine-learning-based methods for tracking **other vessels**: the evaluation metrics and datasets are presented in Section 4; see list of abbreviations at the bottom.

Authors	Methods	Data	Experiment	Results
Bogunović et al. (2012)	SVM, bifurcation features	Internal carotid artery 3DRA, local data	96 images, cross-validation	Cross-validation success rate =0.99
Cheng et al. (2012)	Seed searching	Mammography, local data	1800 samples, 1200 for training, 400 for testing, four-fold cross-validation	Se=0.93, Sp=0.851
Zheng et al. (2012)	Non-rigid deformation, position, orientation and scale	Aorta C-arm CT, local data	319 volumes, four-fold cross-validation	Mean error=1.08 mm
Cherry et al. (2015)	Random forest, intensity, vesselness, ray-casting, MIP, and spanning tree	Pelvis CT angiograms, local data	10 for training, 30 for testing, one-off train + test	Pr=0.7752, Re=0.677
Rempfler et al. (2015)	Probabilistic model, physiological-geometric properties	Mouse brain MR images, local data	4 for training, 1 for testing, leave-one-out	DSC=0.516
Schneider et al. (2015)	Random forest, oriented features	Synthetic vascular data, local data	4 for testing, leave-one-out	DSC=0.95
Zhang et al. (2017b)	Random forest, steerable-frangi-filters and OOF	Perivascular 7T MR, local data	19 image sets, two-fold cross-validation	DSC=0.661, Se=0.651
Lorza et al. (2018)	SVM, a radial basis function kernel	Carotid bifurcation MRI, local data	49 arteries for testing	DSC wall overlap= 0.741

* List of abbreviations: 3DRA=3D rotational angiography; CT=computed tomography; DSC=dice similarity coefficient; MIP=maximum intensity projection; MR=magnetic resonance; MRI=magnetic resonance imaging; OOF=optimally oriented flux; Pr=precision; Re=recall; Se=sensitivity; Sp=specificity.

Table 4
 Overview of the techniques in traditional machine-learning-based methods: see list of abbreviations at the bottom.

Conventional learning-based methods	Techniques
Hand-crafted features	Intensity features: Cherry et al. (2015); Mehmet et al. (2016); Vukadinovic et al. (2010)
	Intensity gradient features: Mehmet et al. (2016)
	Bifurcation feature vectors: Bogunović et al. (2012)
	Spatial location: Mehmet et al. (2016); Vukadinovic et al. (2010)
	Angles: Bogunović et al. (2012); Mehmet et al. (2016)
Learning-based kernels:	Asl et al. (2017); Lesage et al. (2016); Liu et al. (2014); Poletti and Grisan (2014)
	Annunziata et al. (2015a); Azzopardi and Petkov (2013); Lin et al. (2012); Sironi et al. (2015)
Learning-based filters:	Annunziata and Trucco (2016); Deng et al. (2018); Javid et al. (2017); Zhang et al. (2017b)
	Coates and Ng (2012); Saffarzadeh et al. (2014); Samuel et al. (2017); Zhang et al. (2014)
K-means:	Goceri et al. (2017); Lu et al. (2017); Xia et al. (2018)
Fuzzy C-means clustering:	Khan and NaliniPriya (2016); Mapayi and Tapamo (2016); Mapayi et al. (2015)
	Haddad et al. (2018); Zeng et al. (2018)
Support Vector Machine:	A. Osareh (2009); Chen et al. (2015); Hanaoka et al. (2015); You et al. (2011)
	Jawaid et al. (2017); Kang et al. (2015); Lorza et al. (2018); Orlando et al. (2017)
Boosting-based methods:	Gu et al. (2017); Lupascu et al. (2010); Turetken et al. (2016)
	Lupascu et al. (2013); Memari et al. (2017)
	Fraz et al. (2012a); Hashemzadeh and Adlpour Azar (2019); Lupascu et al. (2013)
Random forest:	Annunziata et al. (2015b); Melki et al. (2014); Zhang et al. (2017a)
	Cherry et al. (2015); Sankaran et al. (2016); Schneider et al. (2015)
Hybrid classifiers:	Chapman et al. (2015); Hu et al. (2018b); Lugauer et al. (2014); Rani et al. (2016)
	Cheng et al. (2012); Vukadinovic et al. (2010)
Intensity/appearance model:	Rempfler et al. (2014); Schaap et al. (2011); Zheng et al. (2012)
	Asl et al. (2017); Rempfler et al. (2015); Zhao et al. (2017)
Topological model:	Chai et al. (2013); Kalaitie and Gooya (2017)

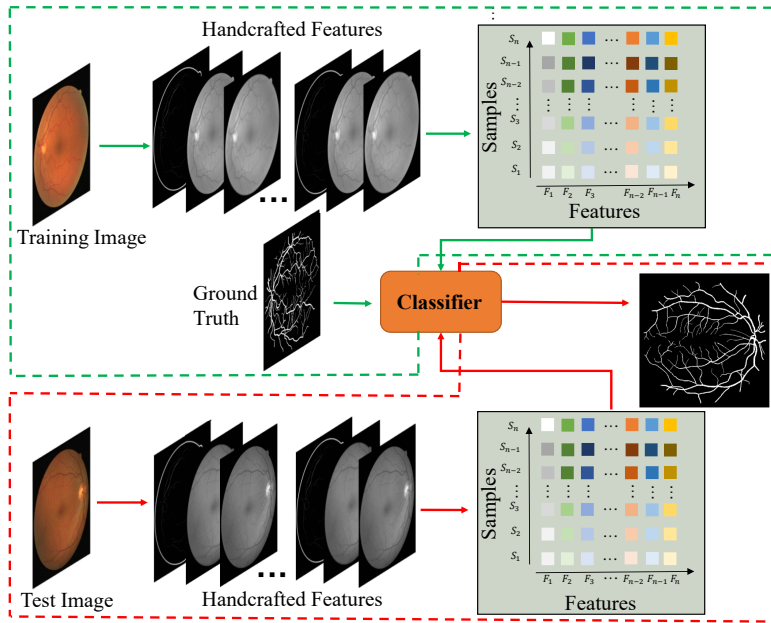


Fig. 2. Diagram of the retinal vessel segmentation using the conventional machine-learning method with supervised training.

Another application is the learning-based filters of vessels. Assuming that the vessel properties changed constantly, Lin et al. (2012) learned the continuity pattern of the current segment using the extended Kalman filter. Azzopardi and Petkov (2013) learned the appropriate prototype features in the filter-configuration process. In addition to the appearance features of learning filters, Annunziata et al. (2015a) introduced the context information (i.e., relationships among objects) in the filter-learning process. The authors assumed that the learned context filters had two clear advantages: incorporating high-level information and obtaining high efficiency and adaptability. To accelerate the learning process, Sironi et al. (2015) computed the filters by linearly combining them with a smaller number of separable filters. This operation can considerably address the problem of the computational complexity at no extra cost in terms of performance. Annunziata and Trucco (2016) proposed a warm-start strategy to solve this problem. This strategy is based on carefully designing hand-crafted filters and modeling appearance properties of curvilinear structures, which are then refined by convolutional sparse coding. Using vascular filters (e.g., Frangi filter and optimally oriented flux), Zhang et al. (2017b) extracted the corresponding types of vascular features and integrated these feature responses into a structured random forest to classify voxels into positive and negative classes. Deng et al. (2018) named all the features for the random forest (RF) as discriminative integrated features. These features are classified as low-level features, vascular features, context features, and local self-similarity descriptor. In addition to the kernels and filters, Javidi et al. (2017) constructed two separate dictionaries to learn the vessel and non-vessel representations. These learned dictionaries yield a strong representation containing the semantic concepts of the image.

2.2. Classifications

The conventional machine-learning-based methods obtain vessels using classifiers. For vessel-tracking tasks, the methodologies of classification can be broadly categorized into the unsupervised and supervised learning strategies.

Unsupervised learning-based methods train the classifier without using labeled vessel data or explicitly using any supervised classification techniques. To separate related regions, seeds and patches, the main schemes reported in the literature are clustering techniques (e.g., k-means and fuzzy C-means). Instead of explicitly obtaining sparse representations, k-means clustering tends to discover sparse projections of the data (Coates and Ng, 2012). As a pre-processing step, the k-means algorithm can be used to partition the pixels into several clusters; e.g., three clusters of related regions (Saffarzadeh et al., 2014) or five groups of images (Zhang et al., 2014). In the process, Samuel et al. (2017) employed the k-means algorithm with subtractive clustering to separate the vessel regions in the image according to the gray-scale intensity. The k-means algorithm is also used for the final refinement of vessel segmentation (Goceri et al., 2017). In addition to vessel regions, Lu et al. (2017) used the manually annotated seeds to represent the vascular features and utilized k-means clustering to exclude the wrong seeds. To find the representative patches from numerous candidate patches, Xia et al. (2018) used k-means clustering to group the patches under the Euclidean distance metric. Fuzzy C-means clustering is another unsupervised learning method for pattern recognition that employs various image properties for separation. Image pixel intensities are not mutually independent; hence, Kande et al. (2010) used a thresholding technique based on the spatially weighted fuzzy C-means algorithm, which can well preserve the spatial structures in a binarized/thresholded image. In (Mapayi et al., 2015), phase-congruency (Kovesi, 1999) has been used to preserve the features with in-phase frequency compo-

nents, and fuzzy C-means clustering is performed for accurate retinal vessel segmentation. [Mapayi and Tapamo \(2016\)](#) further investigated the difference image with fuzzy C-means for the detection of vessels in the retinal image. An improved fuzzy C-means clustering in ([Khan and NaliniPriya, 2016](#)) was also used for pixel classification based on the texture features. Using the contrast-time curve of the pixel as inputs, [Haddad et al. \(2018\)](#) separated the major vessels from the capillary blush and background noise through fuzzy C-means clustering. [Zeng et al. \(2018\)](#) constructed the intensity model based on kernel fuzzy C-means to extract the intensity feature of thick vessels.

The ground truth is absent; hence, the performance of unsupervised methods relies on particular features based on the statistical distribution of the overall input data. In contrast, supervised learning methods require a manually annotated set of training images for classifications. The extracted features and ground truth of every sample are collected to train the classifier. Most of these methods in the supervised category use various classifiers (Fig. 2)—support vector machine (SVM), boosting-based methods, and random forests—to distinguish the vascular patterns in the images.

The SVM classifier performs vessel or non-vessel classification by constructing an N-dimensional hyperplane that optimally separates the vessel samples into different categories. The classification ability of the SVM is based on the feature vectors obtained by different operators and vascular-dedicated filters. The operators can be line operator ([Ricci and Perfetti, 2007](#)), Gabor filters ([A. Osareh, 2009](#)), and wavelets ([You et al., 2011](#)). The vascular-dedicated filters can be Frangi filter ([Frangi et al., 1998](#)) and optimally oriented flux ([Law and Chung, 2010](#)). To distinguish between the vessels, the feature vectors can also be formulated via general measures; e.g., distance between adjacent nodes ([Hanaoka et al., 2015](#)), geometric shapes ([Kang et al., 2015](#)), and normal cross-sections ([Jawaid et al., 2017](#)). To deal with more complex cases in the curve detection, [Chen et al. \(2015\)](#) utilized the joint feature representations—e.g., smoothness of points and position relationships—for classification. Instead of classifying the pixels, in the framework of the fully connected conditional random field (CRF), the SVM methods are employed to adjust the weight parameters in the energy function ([Orlando et al., 2017](#)). [Lorza et al. \(2018\)](#) used the SVM with a radial basis function kernel to obtain the probability map of the vessel region.

Boosting-based methods are dependent on building strong classification models from a linear combination of weak classifiers, making the training easier and faster. Simple functions, such as regression stumps, can be employed in boosting-based methods to detect curvilinear objects ([Turetken et al., 2016](#)). In vessel-segmentation tasks, a regression stump is a decision tree with two terminal nodes. For a given vascular feature, the tree selects a branch according to the threshold based on a binary decision function. As a special case of boosting-based methods, the AdaBoost learning model is trained to automatically detect the bifurcation points of vessels with elaborately selected features. To improve the accuracy of classifications, numerous filters are necessary to obtain the vascular features ([Zhou et al., 2007](#)). [Lupascu et al. \(2010\)](#) used feature vectors, which

are composed of eight elements including the output of filters, measures, and other transformation results, to encode vascular information on the local intensity structure, spatial properties, and geometry at multiple scales. [Gu et al. \(2017\)](#) constructed boosting-tree methods based on features such as variable sizes and locations. These features represent the encoded global contextual information (e.g., context distance and local spatial label patterns). [Memari et al. \(2017\)](#) completed the segmentation based on feature extraction and selection steps, along with the AdaBoost classifier. If a classification tree has an AdaBoost classifier at each node, then the tree will be the probabilistic boosting-tree (PBT) classifier. [Zheng et al. \(2011\)](#) exploited the PBT to identify the pixel inside the vessel using 24 feature vectors from the Hessian matrix. To improve the performance of retinal segmentation methods in the presence of lesions, an ensemble classifier of boosted ([Freund and Schapire, 1995](#)) and bagged decision trees ([Breiman, 1996](#)) has been proposed to manage the healthy and pathological retinal images via several encoded features ([Fraz et al., 2012a](#)). The ensembles of bagged decision trees have also been employed to learn the mapping between vessel widths and corresponding points ([Lupascu et al., 2013](#)). In ([Hashemzadeh and Adlpour Azar, 2019](#)), a root-guided decision tree was used to distinguish between the vessel and non-vessel regions.

A collection of tree-structured classifiers can be assembled as an RF classifier. Different from the SVM and decision trees, the RF ([Cutler et al., 2001](#); [Zhang et al., 2016](#)) tends to deliver high performance because of the embedded feature selection in the model-generation process. In the vessel-tracking process, the selected features are invariably related to the intensity profile or vascular shapes (e.g., tubular structures ([Annunziata et al., 2015b](#); [Melki et al., 2014](#); [Zhang et al., 2017a](#)), vessel center ([Schneider et al., 2015](#)), and tree-like structures ([Sankaran et al., 2016](#))). To cover more features for the RF classifier, researchers used multiple techniques to generate representations in various spaces. [Cherry et al. \(2015\)](#) used two sets of features to distinguish the abnormal vessels: vessel cues and local information.

To improve the performance and avoid the over-fitting problems, hybrid classifiers are used for vessel-classification problems. [Rani et al. \(2016\)](#) combined the SVM and tree-bagger techniques to distinguish between the vessel and non-vessel structures. The works of [Lugauer et al. \(2014\)](#) and [Chapman et al. \(2015\)](#) used the RF, PBT, and logistic regression classifier to identify the lumen contours and edges of vessels. [Hu et al. \(2018b\)](#) intricately applied the cascade-AdaBoost-SVM classifiers to delineate the vessel boundaries.

2.3. Statistical models

The profiles of intensity and geometries of vessels can be learned using statistical models. [Vukadinovic et al. \(2010\)](#) determined the vessel calcium object threshold by simply observing the calcium objects disappear in the image dataset; this threshold is used to segment the calcium regions of the vessels. In ([Cheng et al., 2012](#)), the vessel center threshold, which is referred to as the strong peak near the center of the profile, was learned from a set of manually-labeled samples of parallel

linear structures. For more detailed information, [Schaap et al. \(2011\)](#) learned the local point distribution models and a non-linear boundary intensity model by statistically analyzing the set of annotated training data. [Zheng et al. \(2012\)](#) divided the vessel model into four structures, each of which is recognized via learned detectors. Instead of designing individual classifiers for each geometrical constraint, [Rempfler et al. \(2014\)](#) simply learned the global statistic of the desired geometrical properties of the network from the dataset.

Based on the probabilistic model, the topological structures of vessels, e.g., branches and connections, can also be learned for vessel tracking. [Rempfler et al. \(2015\)](#) learned the physiological geometric properties of vessels such as the relative frequencies of radii and deviation angles of vessel segments. [Asl et al. \(2017\)](#) learned these relationships using kernels. [Zhao et al. \(2017\)](#) learned the topological tree and geometrical statistics of parameters including tree hierarchy, branch angle, and length statistics. Contrary to the pixel-based and object-based methods, [Chai et al. \(2013\)](#) modeled the vessel connections using graph theory. To describe the shape of the graph, they constructed three sets of parameters: graph connectivity, edge orientation, and line width. These parameters can be learned from annotated image samples through a maximum likelihood estimation. Considering the intensity distributions, [Kalaie and Gooya \(2017\)](#) developed a directed probabilistic graphical model whose hyperparameters are estimated using a maximum likelihood solution based on Laplace approximation.

3. Vessel tracking based on deep learning

Using deep-learning-based methods, deep neural networks can be developed to map the input data into vascular patterns such as center points and vascular regions. These patterns can be used to obtain the vessels directly or indirectly. To this end, various deep-learning techniques have been proposed. This section reviews the deep-learning-based methods from three aspects: frameworks of vessel tracking (Section 3.1), architecture of deep neural networks (Section 3.2), and model training (Section 3.3). Tables 5 - 7 summarize the decompositions of a selection of works which are representative of the main trends in the field according to the applications. Table 8 summarizes the existing deep-learning-based works by grouping them into different subcategories.

3.1. Frameworks of vessel tracking

Vessel tracking can be achieved using hierarchical features via a unified framework or a two-step processing scheme. The unified vessel-tracking methods are implemented by integrating feature extraction and pixel classification into one network. In contrast, the two-step scheme generally employs a conventional method to track the vessel based on the preceding vessel features extracted using a deep convolutional neural network (CNN).

The unified framework of vessel tracking can be transformed into resolving a classification or regression problem via the fully connected layers of CNN. The output neurons of CNN that are generally connected to the fully connected layers of the network

determine the labels of pixels. To separate vascular regions from the background using CNN, two neurons are typically set as output layers, following the fully connected layers ([Dasgupta and Singh, 2017](#); [Hu et al., 2017](#); [Liskowski and Krawiec, 2016](#); [Marques et al., 2016](#); [Oliveira et al., 2017](#)). More neurons are output simultaneously to segment vessels and other structures ([Maninis et al., 2016](#); [Tan et al., 2017](#)); this can be regarded as multi-task learning. The idea of multiple tasks has been extended in ([Lahiri et al., 2017](#)), where a discriminator-classifier network differentiates between fake and real vessel samples and assigns correct class labels. The neurons of fully connected layers in conventional CNNs have large receptive fields of input; hence, the results are extremely coarse in the pixel-level vessel segmentation. To resolve the problem, [Li et al. \(2016\)](#) improved the coarse results of conventional CNNs by outputting label maps of the same size. A pixel in the label maps can be affected by the multiple image patches in its neighborhood. This idea is similar to the fully connected CRF, which considers the relationships among the neighbor pixels. To achieve vessel segmentation, the CRF layers can also be used after using the convolutional layers ([Fu et al., 2016a](#); [Luo et al., 2017](#)).

The vessel-tracking process can be divided into two steps: feature learning and vessel tracking. In feature learning, the CNN maps the input image into intermediate representations located between the input and tracking results; e.g., probability maps ([Khowaja et al., 2016](#); [Mou et al., 2019](#); [Nasr-Esfahani et al., 2016](#); [Wolterink et al., 2019](#); [Wu et al., 2016](#)), geometric priors ([Cherukuri et al., 2020](#)), and other feature maps ([Wang et al., 2015](#)). In vessel tracking, the conventional tracking method can be applied to these intermediate representations. The simple approach to complete the tracking is thresholding the probability map ([Mo and Zhang, 2017](#); [Nasr-Esfahani et al., 2018, 2016](#)). [Wang et al. \(2015\)](#) employed ensemble RFs to classify the vascular pixels based on the output feature maps from the selected layers of CNN. [Guo et al. \(2018\)](#) used a voting scheme to determine the results obtained by the CNN. [Mou et al. \(2019\)](#) performed vessel tracking by integrating the predicted probability maps and local vessel directions into the regularized walk algorithm. To refine the results of CNNs, [Hu et al. \(2018a\)](#) added CRF modules at the end of the network and [Chu et al. \(2013\)](#) used the rank-1 tensor-approximation approach to complete the tracking. Inspired by the label-propagation steps of registration methods, [Lee et al. \(2019\)](#) employed a CNN to learn the deformations between the source and the target vessels. The authors assumed that this template transformer network can provide guarantees on the resulting shapes of vessels.

3.2. Network architectures

In vessel-tracking tasks, the CNNs are widely adopted for identifying hierarchical vascular features. To design an effective CNN for the recognition of vascular patterns, two aspects require thorough investigation: network components and integration of multiple networks.

3.2.1. Network components

A CNN is composed of a series of layers (Fig. 3), typically including the convolutional layers, pooling layers, and

Table 5 Overview of deep-learning-based methods for tracking **retinal vessels**; the evaluation metrics and datasets are presented in Section 4; see list of abbreviations at the bottom.

Authors	Methods	Data	Experiment	Results
Li et al. (2016)	Encoder-decoder, 2D	Retinal colored image, DRIVE Retinal colored image, STARE Retinal colored image, CHASE-DB1	20 for training, 20 for testing, one-off train + test 19 for training, 1 for testing, leave-one-out 20 for training, 8 for testing, one-off train + test	Acc=0.9527, AUC=0.9738, Se=0.7569, Sp=0.9816 Acc=0.9628, AUC=0.9879, Se=0.7726, Sp=0.9844 Acc=0.9581, AUC=0.9716, Se=0.7507, Sp=0.9793
Liskowski and Krawiec (2016)	CNN without pooling, 2D	Retinal colored image, DRIVE Retinal colored image, STARE	20 for training, 20 for testing, one-off train + test 19 for training, 1 for testing, leave-one-out	Acc=0.9495, AUC=0.9720 Acc=0.9566, AUC=0.9785
Lahiri et al. (2017) Costa et al. (2018)	GAN, 2D GANs, 2D	Retinal colored image, DRIVE Retinal colored image, DRIVE	20 for training, 20 for testing, one-off train + test 20 for training, 20 for testing, one-off train + test	AUC=0.962 AUC=0.841
Guo et al. (2018)	Multiple CNNs, 2D	Retinal colored image, DRIVE Retinal colored image, STARE	20 for training, 20 for testing, one-off train + test 20 for testing	Acc=0.9597, AUC=0.9726 Acc=0.9613, AUC=0.9737
Yan et al. (2018)	Encoder-decoder, 2D	Retinal colored image, DRIVE Retinal colored image, STARE Retinal colored image, CHASE-DB1	20 for training, 20 for testing, one-off train + test 19 for training, 1 for testing, leave-one-out 20 for training, 8 for testing, one-off train + test	Acc=0.9542, AUC=0.9752, Se=0.7653, Sp=0.9818 Acc=0.9612, AUC=0.9801, Se=0.7581, Sp=0.9846 Acc=0.9610, AUC=0.9781, Se=0.7633, Sp=0.9809
Wu et al. (2018)	Multiple CNNs, 2D	Retinal colored image, DRIVE Retinal colored image, CHASE-DB1	5 for training, 40 for testing, one-off train + test 20 for training, 20 for testing, one-off train + test 20 for training, 8 for testing, one-off train + test	Acc=0.9437, Pt=0.6647, Se=0.7881, Sp=0.9592 Acc=0.9567, AUC=0.9807, Se=0.7844, Sp=0.9819 Acc=0.9637, AUC=0.9825, Se=0.7538, Sp=0.9847
Zhao et al. (2018b)	GANs, 2D	Retinal colored image, DRIVE Retinal colored image, STARE Retinal colored image, HRF	20 for training, 20 for testing, one-off train + test 10 for training, 10 for testing, one-off train + test 22 for training, 23 for testing, one-off train + test	Se=0.8038, Sp=0.9815 Se=0.7896, Sp=0.9841 Se=0.8001, Sp=0.9823
Zhang and Chung (2018)	U-net, 2D	Retinal colored image, DRIVE Retinal colored image, STARE Retinal colored image, CHASE-DB1	20 for training, 20 for testing, one-off train + test 15 for training, 5 for testing, four-fold cross-validation 21 for training, 7 for testing, four-fold cross-validation	Acc=0.9504, AUC=0.9799, Se=0.8723, Sp=0.9618 Acc=0.9712, AUC=0.9882, Se=0.7673, Sp=0.9901 Acc=0.9770, AUC=0.9900, Se=0.7670, Sp=0.9909
Gu et al. (2019)	Context encoder network	Retinal colored image, DRIVE	20 for training, 20 for testing, one-off train + test	Acc=0.955, AUC=0.978
Jin et al. (2019)	Deformable U-net, 2D	Retinal colored image, DRIVE Retinal colored image, STARE Retinal colored image, CHASE-DB1	20 for training, 20 for testing, one-off train + test 19 for training, 1 for testing, leave-one-out 14 for training, 14 for testing, one-off train + test 15 for training, 30 for testing, one-off train + test	Acc=0.9566, AUC=0.9802, TNR=0.9800, TPR=0.7963 Acc=0.9641, AUC=0.9832, TPR=0.7595, TNR=0.9878 Acc=0.9610, AUC=0.9804, TNR=0.9752, TPR=0.8155 Acc=0.9651, AUC=0.9831, TNR=0.9874, TPR=0.7464
Lian et al. (2019)	U-net, Res-net and attention scheme, 2D	Retinal colored image, DRIVE Retinal colored image, STARE	20 for training, 20 for testing, one-off train + test 10 for training, 10 for testing, one-off train + test	Acc=0.9692, Pt=0.8637, Se=0.8278, Sp=0.9861 Acc=0.9740, Pt=0.8823, Se=0.8342, Sp=0.9916
Mou et al. (2019)	Dense dilate network, 2D	Retinal colored image, DRIVE Retinal colored image, STARE Retinal colored image, CHASE-DB1	20 for training, 20 for testing, one-off train + test 15 for training, 5 for testing, four-fold cross-validation 21 for training, 7 for testing, four-fold cross-validation	Acc=0.9594, AUC=0.9796, Se=0.8126, Sp=0.9788 Acc=0.9685, AUC=0.9858, Se=0.8391, Sp=0.9769 Acc=0.9637, AUC=0.9812, Se=0.8268, Sp=0.9773
Shin et al. (2019)	CNN + GNN, 2D	Retinal colored image, DRIVE Retinal colored image, STARE Retinal colored image, CHASE-DB1	20 for training, 20 for testing, one-off train + test 10 for training, 10 for testing, one-off train + test 20 for training, 8 for testing, one-off train + test 15 for training, 30 for testing, one-off train + test	Acc=0.9271, AUC=0.9802, Se=0.9382, Sp=0.9255 Acc=0.9378, AUC=0.9877, Se=0.9598, Sp=0.9352 Acc=0.9373, AUC=0.9830, Se=0.9463, Sp=0.9364 Acc=0.9349, AUC=0.9838, Se=0.9546, Sp=0.9329
Cherukuri et al. (2020)	CNN + geometric prior, 2D	Retinal colored image, DRIVE Retinal colored image, STARE Retinal colored image, CHASE-DB1	20 for training, 20 for testing, four-fold cross-validation 10 for training, 10 for testing, one-off train + test 14 for training, 14 for testing, one-off train + test	Acc=0.9563, AUC=0.9814 Acc=0.9687, AUC=0.9903 Acc=0.9672, AUC=0.9833
Ding et al. (2020b)	Pre-trained model, vessel maps, and noise label, 2D	Retinal UWF FP, PRIME-FP20	15 images, four-fold cross-validation	AUCPR=0.842, Max DSC=0.772

* List of abbreviations: Acc=accuracy; AUC=area under the ROC curve; CNN=convolutional neural networks; GAN=generative adversarial network; GNN=graph neural network; Pt=precision; Re=recall; Se=sensitivity; Sp=specificity; TNR=true negative rate; TPR=true positive rate; UWF FP=ultra-widefield fundus photography.

Table 6 Overview of deep-learning-based methods for tracking **coronary vessels**: the evaluation metrics and datasets are presented in Section 4; see list of abbreviations at the bottom.

Authors	Methods	Data	Experiment	Results
Lee et al. (2019)	CNN + Shape prior, 3D	Coronary CTA, local data	274 for training, 136 for testing, one-off train + test	DSC=0.768, HD=3.55mm
Shin et al. (2019)	CNN + GINN, 2D	Coronary x-ray, CA-XRA (local data)	2958 for training, 179 for testing, one-off train + test	Acc=0.9517, AUC=0.9914, Se=0.9700, Sp=0.9507
Wolterink et al. (2019)	CNN with dilated-convolution, 3D	Coronary CTA, CAT08 Coronary CTA, UMCU dataset (local data) Coronary CTA, orCaScore	7 for training, 1 for testing, leave-one-out 8 for training, 50 for testing, one-off train + test 8 for training, 36 for testing, one-off train + test	AI=0.21mm, OF=0.815, OT=0.970, OV=0.937 Median of radius=0.81mm Visual check

* List of abbreviations:

* Acc=accuracy; AI=average inside; AUC=area under the ROC curve; CNN=convolutional neural networks; CTA = computed tomography angiography; GNN=graph neural network; DSC=dice similarity coefficient; HD=hausdorff distance; Se=sensitivity; Sp=specificity; OF=overlap until first error; OT=overlap with the clinically relevant part of the vessel; OV =overlap.

Table 7

Overview of deep-learning-based methods for tracking **other vessels**: the evaluation metrics and datasets are presented in Section 4; see list of abbreviations at the bottom.

Authors	Methods	Data	Experiment	Results
Marques et al. (2016)	U-net, 3D	Multiple organs, CT, MR, local data	67 for training, 19 for testing, one-off train + test	Pr=0.362
Huang et al. (2018)	Unet, 3D	Liver contrast-enhanced CT, 3D-IRCADb Liver CT, SLIVER07 Liver CT, local data	10 for training, 10 for testing, one-off train + test 20 for testing 10 for testing	DSC=0.675, Se=0.743 Visual check Visual check
Lian et al. (2018)	Modified U-net, 2D	Perivascular spaces, 7T MR, local data	6 for training, 14 for testing, one-off train + test	DSC=0.77, PPV=0.83, Se=0.74
Nardelli et al. (2018a)	CNN + graph cut, 3D	Pulmonary CT, local data	4 for training, 16 for validation	Acc=0.87
Kitrungratsakul et al. (2019)	DensNet, 2.5D	hepatic MR, IRCAD hepatic MR, VASCUSYNTH	19 for training, 1 for testing, leave-one-out 9 for training, 1 for testing, leave-one-out	DSC=0.903, Se=0.929 DSC=0.901
He et al. (2020)	Auto-encoder + dense bias connection, 3D	Renal artery, CT, local data	52 for training, 104 for testing, one-off train + test	DSC=0.884, HD=25.439mm
Nazir et al. (2020)	CNN + dilated-convolution, 3D	Intracranial vessel, CTA, local data	50 for training, 20 for testing, one-off train + test	DSC=0.8946, HD=5.04mm
Ni et al. (2020)	CNN + channel attention	Intracranial vessel, CTA, local data	9488 slices for training, 480 images for testing	DSC=0.965

* List of abbreviations: Acc=accuracy; CNN=convolutional neural networks; CT=computed tomography; CTA = computed tomography angiography; DSC= dice similarity coefficient; HD=hausdorff distance; IRCAD: <http://www.ircad.fr>; MR=magnetic resonance; Pr=precision; PPV=positive predictive value; Se=sensitivity; VASCUSYNTH (Jassi, 2010).

Table 8

Overview of techniques in deep-learning-based methods: see list of abbreviations at the bottom.

Deep-learning-based methods	Techniques
	CNN + Dilated convolution: Mou et al. (2019); Nazir et al. (2020); Wolterink et al. (2019)
	CNN + Deformation convolution: Jin et al. (2019)
	CNN + No Pooling: Liskowski and Krawiec (2016); Tetteh et al. (2017)
	CNN + Probability maps: Fu et al. (2016b); Ganin and Lempitsky (2015); Mo and Zhang (2017) Ding et al. (2020b); Hu et al. (2018a); Lin et al. (2019); Uslu and Bharath (2019)
	CNN + Attention mechanism: Li et al. (2019); Lian et al. (2019); Ni et al. (2020); Shen et al. (2019)
	CNN + Skipping/short connection: Feng et al. (2018); Guo et al. (2019)
	CNN + CRF: Fu et al. (2016a); Luo et al. (2017)
	CNN + Prior: Cherukuri et al. (2020); Lee et al. (2019)
Network architectures	Multi-task learning: Maninis et al. (2016); Tan et al. (2017)
	Encoder-decoder: Dasgupta and Singh (2017); Fan and Mo (2017); Li et al. (2016) Gu et al. (2019); He et al. (2020)
	U-net: Fan et al. (2018); Huang et al. (2018)
	Modified U-net: Chen et al. (2018); Kandil et al. (2018); Wang et al. (2019); Zhang et al. (2019) Dharmawan et al. (2019); Girard et al. (2019); Zhang et al. (2019); Zhang and Chung (2018)
	GNN: Shin et al. (2019)
	GANs: Costa et al. (2018); Yu et al. (2019)
	Multiple CNNs: Guo et al. (2018); Wu et al. (2018)
	Contrast/brightness normalization: Liskowski and Krawiec (2016); Vega et al. (2015)
Pre-processing:	Whiting: Liskowski and Krawiec (2016); Marques et al. (2016)
	Augmentation: Fan et al. (2018); Guo et al. (2019); Huang et al. (2018) Lin et al. (2019); Livne et al. (2019); Zreik et al. (2018)
	Patch as samples: Nardelli et al. (2018b); Wolterink et al. (2019)
Sampling strategies	Image as samples; Hu et al. (2018a); Mo and Zhang (2017)
	Processed image as samples: Hajabdollahi et al. (2018); Nardelli et al. (2017, 2018a) Zhao et al. (2018a); Zreik et al. (2018)
	Loss based on cross-entropy: Dasgupta and Singh (2017); Jin et al. (2019); Nardelli et al. (2018b); Wu et al. (2018) Dharmawan et al. (2019); Guo et al. (2019); Lin et al. (2019); Mo and Zhang (2017)
Loss functions:	Loss to tackle data imbalance: Hu et al. (2018a); Li et al. (2018); Livne et al. (2019); Zhang and Chung (2018) Huang et al. (2018); Kitrungrotsakul et al. (2019); Lian et al. (2018); Soomro et al. (2019)
	Loss based on squared error: Fan and Mo (2017); Li et al. (2016)
	More complex: Jiang et al. (2019); Yan et al. (2018)

List of abbreviations: CNN=convolutional neural networks; CRF=conditional random field; GAN=generative adversarial network; GNN=graph neural network.

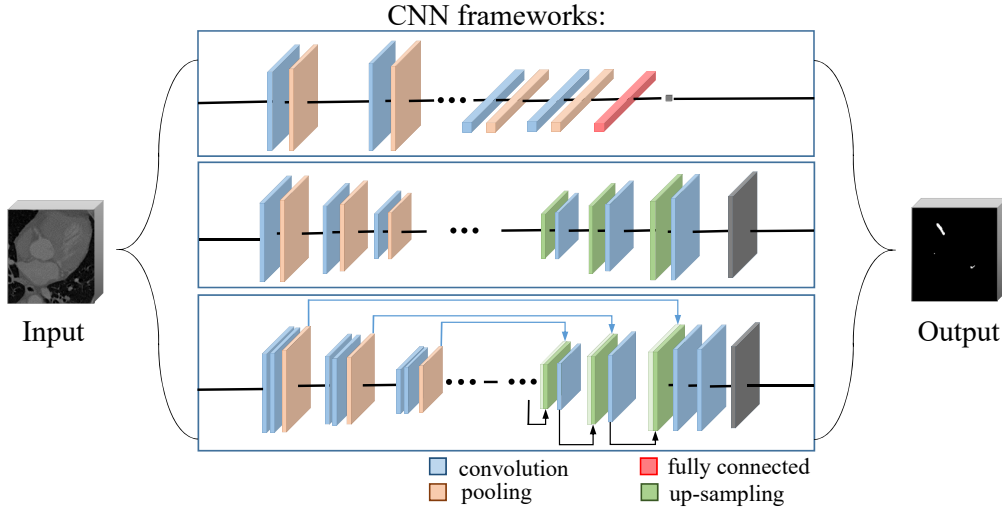


Fig. 3. Illustration of three selected CNN frameworks for the coronary segmentation: pixel-wise CNN (top), encoder-decoder (middle), and U-net (bottom).

fully connected layers. The convolutional and pooling layers are used to build the CNNs in the early applications of vascular feature extraction (Chu et al., 2013), whereas fully connected layers are usually added at the end of a CNN as a part of pixel-classification tasks (Section 2.2). The convolutional layers activate the localized vascular features of the image and feature map by using a set of convolutional units (Nardelli et al., 2018b; Zreik et al., 2018). A stack of dilated convolutions is used in convolutional layers (Mou et al., 2019; Wolterink et al., 2019) to aggregate the features over multiple scales. In addition to dilated convolution modules, Nazir et al. (2020) adopted the inception module fusion of residual connection, enabling the network to capture advanced visual information under a controlled computational complexity. To capture the various shapes and scales of vessels, Jin et al. (2019) integrated the deformation convolution into the network. After the convolution layers, the pooling layers in the CNNs nonlinearly down-sample the input representation and preserve the feature information in each sub-region. The pooling layer aids in reducing the number of parameters irrelevant to the problem (Lian et al., 2018; Nardelli et al., 2018b; Zreik et al., 2018). However, the scaling operation of the pooling layer is considered to rapidly reduce the already extremely limited information contained in the potentially small patch, causing the classification to be more exigent. Therefore, Liskowski and Krawiec (2016) constructed a NO-POOL architecture, which performs well on the datasets. Tetteh et al. (2017) also found that the pooling operations can lead to the loss of fine local details, which are extremely crucial in pixel-wise tasks. To solve this problem, they removed all the pooling layers of the CNN, making the feature-extraction layers robust enough to objects of interest of any size. By employing various size-pooling operations, Gu et al. (2019) used the residual multi-kernel pooling layer that encodes the multi-scale context features without extra learning weights.

Feature maps are organized sets of units obtained through convolution operations. In vessel segmentation, different spatial forms of feature maps can be used in the CNNs. Using

a three-dimensional (3D) CNN, Jin et al. (2017) generated 3D feature maps to learn the structure variations in the 3D space. They assumed that 3D spatial information (especially the 3D branch-level continuity) and junction-bifurcating patterns are important for segmenting vascular structures. Owing to high computational demands, they selected a relatively small region of interest (ROI) and trimmed the network. Yun et al. (2019) used a 2.5D CNN, which simultaneously takes three adjacent slices in each of the orthogonal directions, including axial, sagittal, and coronal, to improve the segmentation accuracy. However, they assumed that they could use the 3D CNN to entirely capture the 3D vascular information in its 3D convolutional layers.

The feature maps created in the network can be applied for final vessel-tracking tasks. Ganin and Lempitsky (2015) found that CNNs are insufficient for learning the mapping from the image patch for vessel annotation, leading to a severe underfitting during the training and suboptimal performance during the test period. To resolve this issue, the network maps the input image or patches into intermediate representations using the CNN. In vessel-segmentation tasks, these mapping results may be the probability maps of vessels. By applying the sigmoid activation function to the final convolution layer, the CNN output is converted to the probability values in the foreground and background regions. The final predicted vessel segmentation can be obtained by fusing these probability maps, which describe the probability distributions of vessels and non-vessels. To predict the vessel boundary, Fu et al. (2016b) utilized the full CNN architecture to output the vessel probability map, followed by the CRF, for a binary segmentation. Mo and Zhang (2017) generated a weighted fusion layer by fusing the multi-scale feature maps from each branch output. In their framework, the probability map is computed using sigmoid functions on the fusion of feature maps. Hu et al. (2018a) obtained the probability map using a multi-scale CNN. By fusing the middle layer feature maps, this CNN model fuses richer multi-scale information for comprehensive feature description to learn more

detailed information on the retinal vessels. Uslu and Bharath (2019) produced the probability maps of vessel interior, center-line, and edge locations. The authors assumed that the probability map can better explain the uncertainty and subjectivity of detecting vessels, especially those at the edge locations appearing in the ground truth data. To formulate the vessel segmentation as a style-transfer problem, Ding et al. (2020b) used the binary probability maps as the tentative training data and the style targets. Considering that shallower side-outputs capture rich detailed information, and deeper side-outputs have high-level but fuzzy knowledge, Lin et al. (2019) outputted the feature maps of each intermediate layer using VGGNet (Simonyan and Zisserman, 2015).

3.2.2. Integration of multiple networks

Because the designed forms of feature maps influence the performance of CNNs, feature maps of different layers are fused to further describe the vessels (Fu et al., 2016b; Wang et al., 2015). These feature-map forms can be derived by the various architectures of CNNs. Based on the number of CNNs used in the vessel-segmentation task, the architecture can be designed as a single CNN or multiple CNNs.

A single CNN for vessel tracking can extract meaningful vascular-structures representations; this is regarded as a problem of dimension reduction or sparse coding feature spaces. For this problem, encoder-decoder architectures (Fig. 3) are introduced to encode the hierarchical features. Instead of transforming the input into another space, Li et al. (2016) developed an auto-encoder network to learn the features, which could recover the input. The auto-encoder network can be embedded into the CNNs to extract features, which could manage large inter-anatomy variations and thin structures such as renal arteries (He et al., 2020). Inspired by the auto-encoder network, Fan and Mo (2017) developed an encoder-decoder style network to learn the mapping functions from the images to the vessels. By formulating the vessel-tracking problem as a multi-label inference problem, Dasgupta and Singh (2017) used the encoder-decoder framework to learn the class-label dependencies of neighboring pixels. By employing the skip connections between the encoder and decoder layers, the modified auto-encoder network facilitates the proper memorization of global and local features and alleviates the vanishing gradient problem of deep CNNs. Feng et al. (2018) concatenated different feature maps through a skipping connection. To learn more inherent features from different scales, Guo et al. (2019) further exploited short connections to fuse multiple outputs of side output layers. To fuse multi-scale features, He et al. (2020) employed a dense biased connection that compresses and transmits the feature maps in each layer to every forward layer. The authors assumed that this connection can reduce feature redundancy and maintain the integrity of the information and gradient flows. Shin et al. (2019) used a graph neural network as a unified CNN to learn the vessel structures.

Similar to an encoder-decoder architecture, the U-net (Ronneberger et al., 2015) can extract vascular features using skip connections (Fig. 3). One feature map generated from a lower layer was concatenated to a corresponding higher layer. The U-net has been used to segment the coronary arteries in

X-ray angiograms (Fan et al., 2018) and liver vessels in CT images (Huang et al., 2018). The global contextual information from the low-level features and the spatial details from the previous convolution guide the precise segmentation. Several methods attempt to efficiently extract or fuse vascular features by improving the structures of U-net (Chen et al., 2018; Kandil et al., 2018; Wang et al., 2019). Yan et al. (2018) added two separate branches at the end of U-net to simultaneously train the model with the segment-level and the pixel-wise losses. To improve the robustness and facilitate convergence, Zhang and Chung (2018) applied a residual connection inside each resample block, which added feature maps before the convolution layers. To reduce the over-fitting problems, the elements in the U-net framework were modified; e.g., adding a dropout layer (Dharmawan et al., 2019) and reducing the number of channels (Livne et al., 2019). Zhang et al. (2019) modified the original U-net by applying an additional convolutional layer before implementing concatenation using the corresponding decoder layer. This configuration also aids in transferring low-dimensional features to a higher-dimensional space.

However, the general U-net may fail to extract some minuscule vessels because this feature accumulation is limited by the depth of U-net (Jin et al., 2019); accordingly, modified U-Nets are developed to focus on vascular structures. Jin et al. (2019) developed a deformable CNN to capture various vessel shapes and scales via deformable receptive fields, which are adaptive to input features. To highlight the vessel-like structures, the attention gate (AG) mechanism is introduced into the CNN (Li et al., 2019; Shen et al., 2019). This AG mechanism can highlight salient features and gradually suppress the characteristic response in unrelated background regions without passing multi-level information (Li et al., 2019; Shen et al., 2019). Lian et al. (2019) incorporated a weighted attention mechanism into the U-net framework. Using this mechanism, the network only focuses on the target ROI and eliminates the irrelevant background noise. To better learn the global feature information, Ni et al. (2020) introduced the channel attention mechanism when aggregating high-level and shallow features.

Different from the single CNN framework, multiple CNNs can be jointly adopted in a framework for vessel tracking. These CNNs can be designed according to different views of the image; e.g., three views (sagittal, coronal, and transverse) of patches (Kitrungrotsakul et al., 2017). Guo et al. (2018) employed multiple CNNs as a voted classifier to improve the performance. Zhao et al. (2018a) accomplished the voxel-level vessel segmentation via the hierarchical update of CNNs. The authors assumed that this network absorbed the learning experience of the previous iteration, which gradually transformed a semi-supervised task into a supervised one. Zhang et al. (2019) proposed a more complicated cascade U-net network (i.e., three sub-networks are designed for different detection tasks).

3.3. Training strategies

The successful training of a useful CNN model relies on a series of strategies. It is essential to design a suitable training strategy to ensure that the network can focus on vascular regions. Considering the vascular profiles and features, the train-

ing strategies should be carefully designed while considering the following aspects: pre-processing, sampling strategies, and formulation of loss functions.

3.3.1. Pre-processing

The trained networks tend to perform better on appropriately pre-processed images. The data pre-processing techniques include contrast/brightness normalization, whitening, and augmentation.

The image brightness may vary across the fields of view, affecting the network performance. To resolve this problem, the contrast or brightness normalization abstracts from these fluctuations and further focuses on vessel regions. A Gaussian kernel is used to homogenize the background (Vega et al., 2015). Liskowski and Krawiec (2016) normalized the patches by subtracting the mean and dividing by the standard deviation of its elements.

Similar to principal component analysis (PCA) processing, the whitening processing can remove the universal correlations among the neighbor pixels of the image. These universal correlations are redundant for training the network. Liskowski and Krawiec (2016) used the zero-phase component analysis to process the image data using rotations, resulting in whitened data that are as close as possible to the original data. Whitening pre-processing has also been used in (Marques et al., 2016).

Training a CNN for a computer-vision task requires tens of thousands of natural images. However, for vessel tracking, the number of training images is relatively small, which may cause an over-fitting problem. To solve this problem, data augmentation can increase the number of training samples using image-transformation approaches (e.g., rotation, scaling, flipping, and mirroring). These transformations yield the desired invariance and robustness properties of the resulting network. The augmentation methods vary according to different tasks. Charbonnier et al. (2017) preserved the orientation of patches with four angles and obtained examples using horizontal flipping. In addition to the rotation and flipping used in (Zhao et al., 2018b), scaling and mirror operations were used in (Huang et al., 2018) and (Guo et al., 2019), respectively. Moreover, random elastic deformation was used to deform the training set (Fan et al., 2018; Livne et al., 2019). Zreik et al. (2018) observed the signs of over-fitting when training was implemented without data augmentation. The results in (Lin et al., 2019) show that data augmentation is essential to achieve excellent performance.

The application of generative adversarial networks (GANs) is highly promising augmentation approach (Costa et al., 2018; Yu et al., 2019). By simply sampling a multi-dimensional normal distribution, Costa et al. (2018) employed the encoder-decoder network to generate realistic vessel networks and extend the training samples. Yu et al. (2019) used the shape-consistent GAN to generate synthetic images that maintain the background of coronary angiography and preserve the vascular structures of retinal vessels. This model can transfer the knowledge of the vessel segmentation from a public dataset to an unlabeled dataset.

3.3.2. Sampling strategies

There are two categories of CNNs according to the input: patch-based and image-based networks. The former extracts numerous patches from the image data as training samples of the network, whereas the latter considers the entire image as a training sample.

For patch-based networks, an efficient extraction strategy should be adopted. Nardelli et al. (2018b) extracted the patches from the CT image around the vessel of interest. Wolterink et al. (2019) directly selected the positive and negative samples focused on the vessel centerlines. Instead of extracting the patches, images can be directly inputted into the network to optimize the model; examples can be found in (Hu et al., 2018a; Mo and Zhang, 2017). More flexible, Girard et al. (2019) used a scalable encoding-decoding CNN model that can input either the entire image directly or patches of any size to the network.

In addition to the samples directly extracted from the image, several works selected the training samples from enhanced images to focus on problems originating from vessel tracking. For example, Nardelli et al. (2017, 2018a) extracted patches from the bronchus image enhanced by the scale-space particle approach. Hajabdollahi et al. (2018) trained the CNN on the enhanced gray-scale level image. Zhao et al. (2018a) selected the patches from both the original and tube-level label images. To directly reflect the stenosis of vessels, Zreik et al. (2018) collected the patches from multi-planar reformatted images.

3.3.3. Formulation of loss functions

The CNNs obtain the optimal network weights by optimizing the loss function. The cross-entropy-based loss functions are generally used in vessel-tracking tasks (Dasgupta and Singh, 2017; Dharmawan et al., 2019; Guo et al., 2019; Jin et al., 2019; Lin et al., 2019; Mo and Zhang, 2017; Nardelli et al., 2018b; Wu et al., 2018). However, the vascular regions in the images are considerably smaller than the non-vascular regions, thereby inducing the imbalance problem for loss-function optimization.

Data-imbalance problems occur in image segmentation, where the number of foreground pixels is usually less than background. To resolve the imbalance problem, some researchers formulated weighted schemes for the categorical cross-entropy loss functions (Hu et al., 2018a; Li et al., 2018; Zhang and Chung, 2018). These loss functions incorporate the coefficients to reduce the importance of well-classified examples and focus on problematic samples. Another solution that has been employed is the use of the dice-coefficient-based loss functions (Kitrungsakul et al., 2019; Livne et al., 2019; Soomro et al., 2019). To balance the classes of voxels, weighted schemes of the dice coefficient are employed to formulate the loss functions. Huang et al. (2018) adjusted the penalty weights of misclassified voxels to obtain higher correct classification scores and lower number of misclassified voxels. Lian et al. (2018) employed a tuning parameter to determine whether precision (i.e., positive prediction value) contributes more than recall (i.e., true positive rate or sensitivity) or conversely during the training procedure.

Alternative methods employ the squared error (Fan and Mo, 2017; Li et al., 2016) or more complex formulations as loss functions to train CNNs. Based on the L1 norm, Yan et al.

(2018) generated a joint loss to simultaneously train the model with the vessel-segment-level loss and pixel-wise loss. Jiang et al. (2019) formulated the loss function by adjusting the weights of two parts: cross entropy and L2 norm.

4. Evaluation issues

4.1. Metrics for performance evaluation

The results of vessel tracking can be presented as key points, vessel centerlines, and label images depending on requirements of the clinical applications. The performances of the methods are evaluated by comparing the results with the ground truth. The key points can be checked visually. For the remaining two types of results, two groups of metrics are generally used: overlap metrics and classification metrics.

Overlap metrics are used to evaluate the similarity between the extracted vessels and ground truth. For label images, true positive (TP), true negative (TN), false negative (FN), and false positive (FP), compared with the ground truth, are typically used to evaluate the vessel and non-vessel patterns; these four metrics can be further formulated as accuracy (Acc), sensitivity (Se), specificity (Sp), precision (Pr), recall (Re), positive predictive value (PPV), negative predictive value (NPV), and dice similarity coefficient (DSC (Dice, 1945)). The DSC and the Hausdorff distance (HD) are widely adopted overlap metrics to assess the similarity between label images. For centerlines, the four metrics can be computed according to the point-to-point correspondence between the ground truth and computed centerline. The four metrics can be further formulated as overlap (OV), overlap until the first error (OF), and overlap with the clinically relevant part of the vessel (OT). The average inside (AI) distance can also be used to describe the average distance of connections between two centerlines. The details of the four metrics for assessing vessel centerlines are found in (Schaap et al., 2009).

Classification metrics are derived from the curves (i.e., receiver operating characteristic (ROC) curve and precision-recall curve) to assess a binary classifier system. The area under the receiver operating characteristic curve (AUC) metric can be used to indicate the probability that a classifier will rank a randomly chosen vessel instance higher than it will rank a randomly chosen non-vessel instance. The AUPRC metric, i.e., the area under the precision-recall curve, can also be exploited to evaluate the results of vessel tracking.

4.2. Public datasets and validation strategies

Standard datasets are required for an objective evaluation of vessel-tracking methods. Here, we summarize the challenges and the public datasets related to vessel tracking.

- (1) Retinal vessel segmentation: DRIVE (<http://www.isi.uu.nl/Research/Databases/DRIVE/>)
- (2) Retinal vessel segmentation: STARE (<http://cecas.clemson.edu/~ahoover/stare/>)
- (3) Retinal vessel segmentation: CHASE-DB1 (<http://blogs.kingston.ac.uk/retinal/chasedb1>)
- (4) Retinal vessel segmentation: HRF (Odstrcilik et al., 2013)
- (5) Retinal vessel segmentation: PRIME-FP20 (Ding et al., 2020a)

- (6) Coronary artery stenosis detection: CASDQEF (<http://coronary.bigr.nl/stenoses>)
- (7) Coronary centerline extraction: CAT08 (<http://coronary.bigr.nl/centerlines>)
- (8) Identify coronary calcifications: orCaScore (<https://orcacore.grand-challenge.org/>)
- (9) Coronary segmentation: ASOCA (<https://asoca.grand-challenge.org/>)
- (10) Lung vessel segmentation: VESSEL12 (Rudyanto et al., 2014)
- (11) Liver segmentation: SLIVER07 (<https://sliver07.grand-challenge.org/>)
- (12) Liver vessel segmentation: 3D-IRCADb (<https://www.ircad.fr/research/3d-ircadb-01/>)

To validate the vessel-tracking methods, the dataset is divided into different training and test groups according, e.g., one-off train + test, leave-one-out and k-fold cross-validation. The experiment columns in Tables 1 - 7 present the validation strategies of the selected methods. Moreover, Table 9 presents the public datasets and selected state-of-the-art results.

5. Conclusion and discussion

We have reviewed the recent literature on vessel tracking, particularly those on the methodologies that apply machine learning, including conventional machine-learning and deep-learning algorithms. Instead of reviewing the methods for a single application (e.g., retinal vessel segmentation and coronary centerline extraction) or based on a specific imaging modality (e.g., colored image and CTA), this paper focuses on reviewing the learning-based methods of tracking vessels of various organs in different imaging modalities. Learning-based methods offer the advantages of mapping the input data into representative and discriminative vascular features. Particularly, conventional learning-based methods learn the vessel-dedicated information from numerous hand-crafted features. They can employ different classifiers to distinguish the vessels from an analogous background according to the learnt features. Moreover, these techniques can describe the vessels with learnt vessel-dedicated parameters using statistical models. In contrast, based on various CNN architectures, deep-learning-based methods leverage hierarchical features that can encode global and local vascular structures.

Owing to the complex morphologies of objects and image characteristics, vessel tracking is an exigent task. Thin vessels are not observed in many vessel-segmentation tasks because of their complex structures and small sizes, and to distinguish the small-sized vessels from artifacts and noise, high-quality local textures are required. Moreover, vessels with uncertain branches and tortuosity are difficult to track because of the complex branch connections. More auxiliary information (e.g., key points and orientations) should be obtained to reconstruct these vessels. Specifically, surrounding tissues and image noise may interfere with vessel tracking because of their positions and image intensities. To reduce the interference, a series of pre-processing techniques should be considered.

Table 9

The public datasets and selected results. Please refer to Section 4 for the abbreviations.

Public dataset	Selected Results	Validation strategy
DRIVE	Acc=0.9692 (Lian et al., 2019)	20 for training, 20 for testing, one-off train + test
	AUC=0.9814 (Cherukuri et al., 2020)	20 for training, 20 for testing, five-fold cross-validation
	Se=0.9382 (Shin et al., 2019)	20 for training, 20 for testing, one-off train + test
	Sp=0.9861 (Lian et al., 2019)	20 for training, 20 for testing, one-off train + test
STARE	Acc=0.9740 (Lian et al., 2019)	10 for training, 10 for testing, one-off train + test
	AUC=0.9882 (Zhang and Chung, 2018)	15 for training, 5 for testing, four-fold cross-validation
	Se=0.9598 (Shin et al., 2019)	10 for training, 10 for testing, one-off train + test
	Sp=0.9916 (Lian et al., 2019)	10 for training, 10 for testing, one-off train + test
CHASE-DB1	Acc=0.9770 (Zhang and Chung, 2018)	21 for training, 7 for testing, four-fold cross-validation
	AUC=0.9900 (Zhang and Chung, 2018)	21 for training, 7 for testing, four-fold cross-validation
	Se=0.9463 (Shin et al., 2019)	20 for training, 8 for testing, one-off train + test
	Sp=0.9909 (Lian et al., 2019)	21 for training, 7 for testing, four-fold cross-validation
HRF	Acc=0.9651 (Jin et al., 2019)	15 for training, 30 for testing, one-off train + test
	AUC=0.9838 (Shin et al., 2019)	15 for training, 30 for testing, one-off train + test
	Se=0.9546 (Shin et al., 2019)	15 for training, 30 for testing, one-off train + test
	Sp=0.9823 (Zhao et al., 2018b)	22 for training, 23 for testing, one-off train + test
CAT08	AI=0.21mm (Wolterink et al., 2019)	7 for training, 1 for testing, leave-one-out
	OF=0.815 (Wolterink et al., 2019)	7 for training, 1 for testing, leave-one-out
	OT=0.971 (Schaap et al., 2011)	8 for training, 24 for testing, one-off train + test
	OV=0.969 (Schaap et al., 2011)	8 for training, 24 for testing, one-off train + test

The recent literature on vessel tracking mainly reports the advanced machine-learning methodologies in view of their considerable modeling capacities and potential in extracting effective features. Nevertheless, the following two problems should be considered when a new algorithm for this task is developed.

First, learning-based methods may deliver limited performance in tracking a complete vessel because of the lack of high-level vascular features (e.g., branches and connections). The models can be trained based on hand-crafted features (Section 2) or hierarchical features (Section 3). However, in clinical practice, developing vessel-tracking methods may be exigent because of the problems involved in detecting abnormal vessels or vessels with pathologies. To describe these vessels in detail, the extraction of high-level features for future learning-based tracking methods is required.

The second problem is related to the strategies employed to deal with the limited training data because this insufficiency generally leads to poor generalization capacity of models. Deep learning has achieved considerable success in many applications where public datasets with annotation are available. However, in the field of medical image analysis, overcoming the limitation of training data is still a major challenge. Currently, data augmentation is a common strategy employed to alleviate this issue. Moreover, weakly supervised and self-supervised learning are potential approaches to resolve the problems of lacking annotated data. Hence, in the future, more public databases are expected to be available, such as via open challenges, to promote the learning-based vessel-tracking algorithms.

Acknowledgment

This work was funded by the National Natural Science Foundation of China (grant no. 61971142 and 62011540404) and the development fund for Shanghai talents (no. 2020015)

References

- A. Osareh, B.S., 2009. Automatic blood vessel segmentation in color images of retina. *Iranian Journal Of Science And Technology Transaction B – Engineering* 33, 191–206.
- Abramoff, M.D., Garvin, M.K., Sonka, M., 2010. Retinal imaging and image analysis. *IEEE Reviews in Biomedical Engineering* 3, 169–208.
- Agam, G., Armato, S.G., Wu, C., 2005. Vessel tree reconstruction in thoracic CT scans with application to nodule detection. *IEEE Transactions on Medical Imaging* 24, 486–499.
- Al-Diri, B., Hunter, A., Steel, D., Habib, M., Berry, S., 2008. REVIEW-a reference data set for retinal vessel profiles, in: *International Conference of the IEEE Engineering in Medicine and Biology Society*.
- Annunziata, R., Kheirhah, A., Hamrah, P., Trucco, E., 2015a. Boosting Hand-Crafted Features for Curvilinear Structure Segmentation by Learning Context Filters, in: *Medical Image Computing and Computer-Assisted Intervention*, Pt Iii. volume 9351, pp. 596–603.
- Annunziata, R., Kheirhah, A., Hamrah, P., Trucco, E., 2015b. Scale and curvature invariant ridge detector for tortuous and fragmented structures, in: *Medical Image Computing and Computer Assisted Intervention (MICCAI)*, Springer, Cham. pp. 588–595.
- Annunziata, R., Trucco, E., 2016. Accelerating Convolutional Sparse Coding for Curvilinear Structures Segmentation by Refining SCIRD-TS Filter Banks. *IEEE Transactions on Medical Imaging* 35, 2381–2392.
- Asl, M.E., Koohbanani, N.A., Frangi, A.F., Gooya, A., 2017. Tracking and diameter estimation of retinal vessels using Gaussian process and Radon transform. *Journal of Medical Imaging* 4, 1.
- Azzopardi, G., Petkov, N., 2013. Trainable COSFIRE Filters for Keypoint Detection and Pattern Recognition. *IEEE Transactions on Pattern Analysis and Machine Intelligence* 35, 490–503.
- Becker, C., Rigamonti, R., Lepetit, V., Fua, P., 2013. Supervised feature learning for curvilinear structure segmentation. *Medical Image Computing and Computer Assisted Intervention (MICCAI) 8149 LNCS*, 526–533.
- Bogunović, H., Pozo, J.M., Cárdenes, R., Villa-Uriol, M.C., Blanc, R., Píotin, M., Frangi, A.F., Bogunovic, H., Pozo, J.M., Cardenes, R., Villa-Uriol, M.C., Blanc, R., Píotin, M., Frangi, A.F., 2012. Automated landmarking and geometric characterization of the carotid siphon. *Medical Image Analysis* 16, 889–903.
- Breiman, L., 1996. Bagging predictors. *Machine Learning* 24, 123–140.
- Chai, D., Forstner, W., Lafarge, F., 2013. Recovering line-networks in images by junction-point processes. *Proceedings of the IEEE Computer Society Conference on Computer Vision and Pattern Recognition*, 1894–1901.
- Chapman, B.E., Berty, H.P., Schulthies, S.L., 2015. Automated generation of directed graphs from vascular segmentations. *Journal of Biomedical Informatics* 56, 395–405.
- Charbonnier, J.P., Rikxoort, E.M., Setio, A.A., Schaefer-Prokop, C.M., van Ginneken, B., Ciompi, F., 2017. Improving airway segmentation in computed tomography using leak detection with convolutional networks. *Medical Image Analysis* 36, 52–60.

- Chen, J., Li, M., Jin, Q., Bao, S., Su, Z., Yu, Y., 2015. Lead curve detection in drawings with complex cross-points. *Neurocomputing* 168, 35–46.
- Chen, X.H., Lu, Y., Bai, J.J., Yin, Y.B., Cao, K.L., Li, Y.W., Chen, H.B., Song, Q., Wu, J., 2018. Train a 3d u-net to segment cranial vasculature in cta volume without manual annotation, in: 2018 IEEE 15th International Symposium on Biomedical Imaging, pp. 559–563.
- Cheng, J.Z., Chen, C.M., Cole, E.B., Pisano, E.D., Shen, D.G., 2012. Automated Delineation of Calcified Vessels in Mammography by Tracking With Uncertainty and Graphical Linking Techniques. *IEEE Transactions on Medical Imaging* 31, 2143–2155.
- Cherry, K.M., Peplinski, B., Kim, L., Wang, S.J., Lu, L., Zhang, W.D., Liu, J.F., Wei, Z.S., Summers, R.M., 2015. Sequential Monte Carlo tracking of the marginal artery by multiple cue fusion and random forest regression. *Medical Image Analysis* 19, 164–175.
- Cherukuri, V., Bg, V.K., Bala, R., Monga, V., 2020. Deep Retinal Image Segmentation with Regularization under Geometric Priors. *IEEE Transactions on Image Processing* 29, 2552–2567.
- Chu, P., Pang, Y., Cheng, E., Zhu, Y., Zheng, Y., 2013. Structure-Aware Rank-1 Tensor Approximation for Curvilinear Structure Tracking Using Learned Hierarchical Features. *Medical Image Computing and Computer Assisted Intervention (MICCAI)* 8150, 413–421.
- Çimen, S., Gooya, A., Grass, M., Frangi, A.F., 2016. Reconstruction of coronary arteries from X-ray angiography: A review. *Medical Image Analysis* 32, 46–68.
- Coates, A., Ng, A.Y., 2012. Learning Feature Representations with K-Means, 561–580.
- Costa, P., Galdran, A., Meyer, M.I., Niemeijer, M., Abràmoff, M., Mendonça, A.M., Campilho, A., 2018. End-to-End Adversarial Retinal Image Synthesis. *IEEE Transactions on Medical Imaging* 37, 781–791.
- Cutler, A., Cutler, D.R., Stevens, J.R., 2001. Random forests. *Machine Learning* 45, 5–32.
- Dasgupta, A., Singh, S., 2017. A fully convolutional neural network based structured prediction approach towards the retinal vessel segmentation. *Proceedings - International Symposium on Biomedical Imaging*, 248–251.
- Deng, X., Zheng, Y., Xu, Y., Xi, X., Li, N., Yin, Y., 2018. Graph cut based automatic aorta segmentation with an adaptive smoothness constraint in 3D abdominal CT images. *Neurocomputing* 310, 46–58.
- Dharmawan, D.A., Li, D., Ng, B.P., Rahardja, S., 2019. A New Hybrid Algorithm for Retinal Vessels Segmentation on Fundus Images. *IEEE Access* 7, 41885–41896.
- Dice, L.R., 1945. Measures of the amount of ecologic association between species. *Ecology* 26.
- Ding, L., Kuriyan, A.E., Ramchandran, R.S., Wykoff, C.C., Sharma, G., 2020a. PRIME-FP20: Ultra-widefield fundus photography vessel segmentation dataset.
- Ding, L., Kuriyan, A.E., Ramchandran, R.S., Wykoff, C.C., Sharma, G., 2020b. Weakly-supervised vessel detection in ultra-widefield fundus photography via iterative multi-modal registration and learning. *IEEE Transactions on Medical Imaging*, 1–1.
- Fan, J., Yang, J., Wang, Y., Yang, S., Ai, D., Huang, Y., Song, H., Hao, A., Wang, Y., 2018. Multichannel Fully Convolutional Network for Coronary Artery Segmentation in X-Ray Angiograms. *IEEE Access* 6, 44635–44643.
- Fan, Z., Mo, J.J., 2017. Automated blood vessel segmentation based on denoising auto-encoder and neural network. *Proceedings - International Conference on Machine Learning and Cybernetics* 2, 849–856.
- Feng, Z., Yang, J., Yao, L., 2018. Patch-based fully convolutional neural network with skip connections for retinal blood vessel segmentation. *Proceedings - International Conference on Image Processing, ICIP 2017-Septe*, 1742–1746.
- Frangi, A.F., Niessen, W.J., Vincken, K.L., Viergever, M.a., 1998. Multiscale vessel enhancement filtering. *International Conference on Medical Image Computing and Computer-assisted Intervention*, 130–137.
- Fraz, M.M., Barman, S.A., Remagnino, P., Hoppe, A., Basit, A., Uyyanonvara, B., Rudnicka, A.R., Owen, C.G., 2012a. An approach to localize the retinal blood vessels using bit planes and centerline detection. *Computer methods and programs in biomedicine* 108, 600–616.
- Fraz, M.M., Remagnino, P., Hoppe, A., Uyyanonvara, B., Rudnicka, A.R., Owen, C.G., Barman, S.A., 2012b. Blood vessel segmentation methodologies in retinal images—A survey. *Computer methods and programs in biomedicine* 108, 407–433.
- Freund, Y., Schapire, R.E., 1995. A decision-theoretic generalization of on-line learning and an application to boosting, pp. 23–37.
- Fu, H., Xu, Y., Lin, S., Wing, D., Wong, K., Liu, J., 2016a. DeepVessel: Retinal Vessel Segmentation via Deep Learning and Conditional Random Field, in: *Medical Image Computing and Computer Assisted Intervention (MICCAI)*, pp. 132–139.
- Fu, H.Z., Xu, Y.W., Wong, D.W.K., Liu, J., 2016b. Retinal vessel segmentation via deep learning network and fully-connected conditional random fields, in: 2016 IEEE 13th International Symposium on Biomedical Imaging. volume 2016-June, pp. 698–701.
- Ganin, Y., Lempitsky, V., 2015. N4-Fields: Neural Network Nearest Neighbor Fields for Image Transforms. *Asian Conference on Computer Vision 9005*, 536–551.
- Girard, F., Kavalec, C., Cheriet, F., 2019. Joint segmentation and classification of retinal arteries/veins from fundus images. *Artificial intelligence in medicine* 94, 96–109.
- Goceri, E., Shah, Z.K., Gurcan, M.N., 2017. Vessel segmentation from abdominal magnetic resonance images: adaptive and reconstructive approach. *International Journal for Numerical Methods in Biomedical Engineering* 33, 1–16.
- Gu, L., Zhang, X., Zhao, H., Li, H., Cheng, L., 2017. Segment 2D and 3D Filaments by Learning Structured and Contextual Features. *IEEE Transactions on Medical Imaging* 36, 596–606.
- Gu, Z., Cheng, J., Fu, H., Zhou, K., Hao, H., Zhao, Y., Zhang, T., Gao, S., Liu, J., 2019. CE-Net: Context Encoder Network for 2D Medical Image Segmentation. *IEEE Transactions on Medical Imaging* 38, 2281–2292.
- Guo, S., Wang, K., Kang, H., Zhang, Y., Gao, Y., Li, T., 2019. BTS-DSN: Deeply supervised neural network with short connections for retinal vessel segmentation. *International Journal of Medical Informatics* 126, 105–113.
- Guo, Y., Budak, Ü., Şengür, A., 2018. A novel retinal vessel detection approach based on multiple deep convolution neural networks. *Computer Methods and Programs in Biomedicine* 167, 43–48.
- Haddad, C.W., Carroll, T.J., Christoforidis, G.A., Giger, M.L., Haddad, C.W., Drukker, K., Gullett, R., Carroll, T.J., Christoforidis, G.A., Giger, M.L., 2018. Fuzzy c-means segmentation of major vessels in angiographic images of stroke. *Journal of Medical Imaging* 5, 1.
- Hajabdollahi, M., Esfandiarpour, R., Najarian, K., Karimi, N., Samavi, S., Reza-Soroushmeh, S.M., 2018. Low complexity convolutional neural network for vessel segmentation in portable retinal diagnostic devices. *Proceedings - International Conference on Image Processing, ICIP*, 2785–2789.
- Hameeteman, K., Zuluaga, M.A., Freiman, M., Joskowicz, L., Cuisenaire, O., Valencia, L.F., Gülsün, M.A., Krissian, K., Mille, J., Wong, W.C.K., Orkisz, M., Tek, H., Hoyos, M.H., Benmansour, F., Chung, A.C.S., Rozie, S., Gils, M.V., Borne, L.V.D., Sosna, J., Berman, P., Cohen, N., Douek, P.C., Sánchez, I., Aissat, M., Schaap, M., Metz, C.T., Krestin, G.P., Lugt, A.V.D., Niessen, W.J., Walsum, T.V., 2011. Evaluation framework for carotid bifurcation lumen segmentation and stenosis grading. *Medical Image Analysis* 15, 477–488.
- Hanaoka, S., Nomura, Y., Nemoto, M., Miki, S., Yoshikawa, T., Hayashi, N., Ohtomo, K., Masutani, Y., Shimizu, A., 2015. HoTPiG: A Novel Geometrical Feature for Vessel Morphometry and Its Application to Cerebral Aneurysm Detection, pp. 103–110.
- Hashemzadeh, M., Adlpour Azar, B., 2019. Retinal blood vessel extraction employing effective image features and combination of supervised and unsupervised machine learning methods. *Artificial Intelligence in Medicine* 95, 1–15.
- He, Y., Yang, G., Yang, J., Chen, Y., Kong, Y., Wu, J., Tang, L., Zhu, X., Dillenseger, J.L., Shao, P., Zhang, S., Shu, H., Coatrieux, J.L., Li, S., 2020. Dense biased networks with deep priori anatomy and hard region adaptation: Semi-supervised learning for fine renal artery segmentation. *Medical image analysis* 63, 101722.
- Hu, C., Hui, H., Wang, S., Dong, D., Liu, X., Yang, X., Tian, J., 2017. Cerebral vessels segmentation for light-sheet microscopy image using convolutional neural networks. *Medical Imaging 2017: Biomedical Applications in Molecular, Structural, and Functional Imaging* 10137, 101370K.
- Hu, K., Zhang, Z.Z., Niu, X.R., Zhang, Y., Cao, C.H., Xiao, F., Gao, X.P., 2018a. Retinal vessel segmentation of color fundus images using multiscale convolutional neural network with an improved cross-entropy loss function. *Neurocomputing* 309, 179–191.
- Hu, X., Cheng, Y., Ding, D., Chu, D., 2018b. Axis-Guided Vessel Segmentation Using a Self-Constructing Cascade-AdaBoost-SVM Classifier. *BioMed*

Research International 2018, 1–12.

Huang, Q., Sun, J.F., Ding, H., Wang, X.D., Wang, G.Z., 2018. Robust liver vessel extraction using 3D U Net with variant dice loss function. *Computers in Biology and Medicine* 101, 153–162.

Jassi, H.P., 2010. Vascusynth: Simulating vascular trees for generating volumetric image data with ground-truth segmentation and tree analysis. *Computerized Medical Imaging and Graphics*.

Javidi, M., Pourreza, H.R., Harati, A., 2017. Vessel segmentation and microaneurysm detection using discriminative dictionary learning and sparse representation. *Computer Methods and Programs in Biomedicine* 139, 93–108.

Jawaid, M.M., Riaz, A., Rajani, R., Reyes-Aldasoro, C.C., Slabaugh, G., 2017. Framework for detection and localization of coronary non-calcified plaques in cardiac CTA using mean radial profiles. *Computers in Biology and Medicine* 89, 84–95.

Jiang, Y., Tan, N., Peng, T.T., Zhang, H., 2019. Retinal Vessels Segmentation Based on Dilated Multi-Scale Convolutional Neural Network. *IEEE Access* 7, 76342–76352.

Jin, D.K., Xu, Z.Y., Harrison, A.P., George, K., Mollura, D.J., 2017. 3D Convolutional Neural Networks with Graph Refinement for Airway Segmentation Using Incomplete Data Labels, in: *Machine Learning in Medical Imaging*, volume 10541, pp. 141–149.

Jin, Q., Meng, Z., Pham, T.D., Chen, Q., Wei, L., Su, R., 2019. DUNet: A deformable network for retinal vessel segmentation. *Knowledge-Based Systems*.

Kalaie, S., Gooya, A., 2017. Vascular tree tracking and bifurcation points detection in retinal images using a hierarchical probabilistic model. *Computer Methods and Programs in Biomedicine* 151, 139–149.

Kande, G.B., Subbaiah, P.V., Savithri, T.S., 2010. Unsupervised Fuzzy Based Vessel Segmentation In Pathological Digital Fundus Images. *Journal of Medical Systems* 34, 849–858.

Kandil, H., Soliman, A., Taher, F., Mahmoud, A., Elmaghraby, A., El-Baz, A., 2018. Using 3-D CNNs and Local Blood Flow Information to Segment Cerebral Vasculature, in: *2018 IEEE International Symposium on Signal Processing and Information Technology*, pp. 701–705.

Kang, D., Ko, H., Kuo, C.C.J., Dey, D., Li, D., Slomka, P.J., Arsanjani, R., Nakazato, R., Berman, D.S., 2015. Structured learning algorithm for detection of nonobstructive and obstructive coronary plaque lesions from computed tomography angiography. *Journal of Medical Imaging* 2.

Kerrien, E., Yureidini, A., Dequidt, J., Duriez, C., Anxionnat, R., Cotin, S., 2017. Blood vessel modeling for interactive simulation of interventional neuroradiology procedures. *Medical Image Analysis* 35, 685–698.

Khan, K.B., Khaliq, A.A., Jalil, A., Iftikhar, M.A., Ullah, N., Aziz, M.W., Ullah, K., Shahid, M., 2019. A review of retinal blood vessels extraction techniques: challenges, taxonomy, and future trends. *Pattern Analysis and Applications* 22, 767–802.

Khan, Z.F., NaliniPriya, G., 2016. Automatic Segmentation of Retinal Blood Vessels Employing Textural Fuzzy C-Means Clustering.

Khowaja, S.A., Unar, M.A., Ismaili, I.A., Khuwaja, P., 2016. Supervised method for blood vessel segmentation from coronary angiogram images using 7-D feature vector. *Imaging Science Journal* 64, 196–203.

Kirbas, C., Francis, Q., 2004. A Review of Vessel Extraction Techniques and Algorithms. *Computing Surveys* 36, 81–121.

Kirishli, H.A., Schaap, M., Metz, C.T., Dharampal, A.S., Meijboom, W.B., Papadopoulou, S.L., Dedic, A., Nieman, K., de Graaf, M.A., Meijs, M.F.L., Cramer, M.J., Broersen, A., Cetin, S., Eslami, A., Florez-Valencia, L., Lor, K.L., Matuszewski, B., Melki, I., Mohr, B., Oksuz, I., Shahzad, R., Wang, C., Kitslaar, P.H., Unal, G., Katouzian, A., Orkisz, M., Chen, C.M., Precioso, F., Najman, L., Masood, S., Unay, D., Van Vliet, L., Moreno, R., Goldenberg, R., Vucini, E., Krestin, G.P., Niessen, W.J., van Walsum, T., 2013. Standardized evaluation framework for evaluating coronary artery stenosis detection, stenosis quantification and lumen segmentation algorithms in computed tomography angiography. *Medical Image Analysis* 17, 859–876.

Kitrungrotsakul, T., Han, X.H., Iwamoto, Y., Foruzan, A.H., Lin, L., Chen, Y.W., 2017. Robust hepatic vessel segmentation using multi deep convolution network 1013711, 1013711.

Kitrungrotsakul, T., Han, X.H., Iwamoto, Y., Lin, L., Foruzan, A.H., Xiong, W., Chen, Y.W., 2019. VesselNet: A deep convolutional neural network with multi pathways for robust hepatic vessel segmentation. *Computerized Medical Imaging and Graphics* 75, 74–83.

Klepaczko, A., Szczypiński, P., Deistung, A., Reichenbach, J.R., Materka, A., 2016. Simulation of MR angiography imaging for validation of cerebral arteries segmentation algorithms. *Computer Methods and Programs in Biomedicine* 137, 293–309.

Kovesi, P., 1999. Image Features from Phase Congruency. *Journal of computer vision research*, 309–18.

L Srinidhi, C., Aparna, P., Rajan, J., 2017. Recent Advancements in Retinal Vessel Segmentation. *Journal of Medical Systems* 41.

Lahiri, A., Ayush, K., Biswas, P.K., Mitra, P., 2017. Generative Adversarial Learning for Reducing Manual Annotation in Semantic Segmentation on Large Scale Microscopy Images: Automated Vessel Segmentation in Retinal Fundus Image as Test Case. *IEEE Computer Society Conference on Computer Vision and Pattern Recognition Workshops 2017-July*, 794–800.

Law, M.W.K., Chung, A.C.S., 2010. An oriented flux symmetry based active contour model for three dimensional vessel segme, in: *Computer Vision - ECCV*, pp. 720–734.

Lee, M.C.H., Petersen, K., Pawlowski, N., Glocker, B., Schaap, M., 2019. TETRIS: Template Transformer Networks for Image Segmentation with Shape Priors. *IEEE Transactions on Medical Imaging*, 1–1.

Lesage, D., Angelini, E.D., Bloch, I., Funka-Lea, G., 2009. A review of 3D vessel lumen segmentation techniques: Models, features and extraction schemes. *Medical Image Analysis* 13, 819–845.

Lesage, D., Angelini, E.D., Funka-Lea, G., Bloch, I., 2016. Adaptive particle filtering for coronary artery segmentation from 3D CT angiograms. *Computer Vision and Image Understanding* 151, 29–46.

Li, M., Yin, Q., Lu, M., 2018. Retinal Blood Vessel Segmentation Based on Multi-Scale Deep Learning 15, 117–123.

Li, Q., Feng, B., Xie, L., Liang, P., Zhang, H., Wang, T., 2016. A cross-modality learning approach for vessel segmentation in retinal images. *IEEE Transactions on Medical Imaging* 35, 109–118.

Li, R., Li, M., Li, J., 2019. Connection Sensitive Attention U-NET for Accurate Retinal Vessel Segmentation.

Lian, C.F., Zhang, J., Liu, M.X., Zong, X.P., Hung, S.c.C., Lin, W.L., Shen, D.G., 2018. Multi-channel multi-scale fully convolutional network for 3D perivascular spaces segmentation in 7T MR images. *Medical Image Analysis* 46, 106–117.

Lian, S., Li, L., Lian, G., Xiao, X., Luo, Z., Li, S., 2019. A Global and Local Enhanced Residual U-Net for Accurate Retinal Vessel Segmentation. *IEEE/ACM Transactions on Computational Biology and Bioinformatics*, 1–1.

Lin, K.S., Tsai, C.L., Tsai, C.H., Sofka, M., Chen, S.J., Lin, W.Y., 2012. Retinal Vascular Tree Reconstruction With Anatomical Realism. *IEEE Transactions on Biomedical Engineering* 59, 3337–3347.

Lin, Y., Zhang, H.G., Hu, G., 2019. Automatic Retinal Vessel Segmentation via Deeply Supervised and Smoothly Regularized Network. *IEEE Access* 7, 57717–57724.

Liskowski, P., Krzawiec, K., 2016. Segmenting Retinal Blood Vessels With Deep Neural Networks. *IEEE Transactions on Medical Imaging* 35, 2369–2380.

Liu, X.M., Zeng, Z.G., Wang, X.P., 2014. Vessel segmentation in retinal images with a multiple kernel learning based method, in: *Proceedings of the 2014 International Joint Conference on Neural Networks*, pp. 493–497.

Livne, M., Rieger, J., Aydin, O.U., Taha, A.A., Akay, E.M., Kossen, T., Sobesky, J., Kelleher, J.D., Hildebrand, K., Frey, D., Madai, V.I., 2019. A U-Net Deep Learning Framework for High Performance Vessel Segmentation in Patients With Cerebrovascular Disease. *Frontiers in neuroscience* 13, 97.

Lorza, A.M.A., van Engelen, A., Petersen, J., van der Lugt, A., de Bruijne, M., Arias Lorza, A.M., van Engelen, A., Petersen, J., van der Lugt, A., de Bruijne, M., Lorza, A.M.A., van Engelen, A., Petersen, J., van der Lugt, A., de Bruijne, M., Arias Lorza, A.M., van Engelen, A., Petersen, J., van der Lugt, A., de Bruijne, M., 2018. Maximization of regional probabilities using Optimal Surface Graphs: Application to carotid artery segmentation in MRI. *Medical Physics* 45, 1159–1169.

Lu, S., Huang, H., Liang, P., Chen, G., Xiao, L., 2017. Hepatic vessel segmentation using variational level set combined with non-local robust statistics. *Magnetic Resonance Imaging* 36, 180–186.

Lugauer, F., Zhang, J., Zheng, Y., Hornegger, J., Kelm, B.M., 2014. Improving accuracy in coronary lumen segmentation via explicit calcium exclusion, learning-based ray detection and surface optimization. *Medical Imaging 2014: Image Processing* 9034, 90343U.

Luo, Y., Yang, L., Wang, L., B, H.C., 2017. Efficient CNN-CRF Network for

- Retinal Image Segmentation 710, 157–165.
- Lupascu, C.A., Tegolo, D., Trucco, E., 2010. FAB3: Retinal Vessel Segmentation Using AdaBoost. *IEEE Transactions on Information Technology in Biomedicine* 14, 1267–1274.
- Lupascu, C.A., Tegolo, D., Trucco, E., Lupaşcu, C.A., Tegolo, D., Trucco, E., 2013. Accurate estimation of retinal vessel width using bagged decision trees and an extended multiresolution Hermite model. *Medical Image Analysis* 17, 1164–1180.
- Maninis, K.K., Pont-Tuset, J., Arbeláez, P., Van Gool, L., 2016. Deep retinal image understanding. *Lecture Notes in Computer Science (including subseries Lecture Notes in Artificial Intelligence and Lecture Notes in Bioinformatics)* 9901 LNCS, 140–148.
- Manniesing, R., Viergever, M.A., Niessen, W.J., 2006. Vessel enhancing diffusion A scale space representation of vessel structures. *Medical Image Analysis* 10, 815–825.
- Mansour, R.F., 2017. Evolutionary Computing Enriched Computer-Aided Diagnosis System for Diabetic Retinopathy: A Survey. *IEEE Reviews in Biomedical Engineering* 10, 334–349.
- Mapayi, T., Tapamo, J.R., 2016. Difference Image and Fuzzy C-Means for Detection of Retinal Vessels, in: 2016 IEEE Southwest Symposium on Image Analysis and Interpretation, pp. 169–172.
- Mapayi, T., Tapamo, J.R., Viriri, S., 2015. Retinal Vessel Segmentation: A Comparative Study of Fuzzy C-Means and Sum Entropy Information on Phase Congruency. *International Journal of Advanced Robotic Systems* 12, 133.
- Marques, C., Ramalho, J.S., Pereira, P., Mota, M.C., 2016. Dense Volume-to-Volume Vascular Boundary Detection. *International Conference on Medical Image Computing and Computer-assisted Intervention* 90, 371–279.
- Mehmet, A.G., Gülsün, M.A., Funka-Lea, G., Sharma, P., Rapaka, S., Zheng, Y., 2016. Coronary Centerline Extraction via Optimal Flow Paths and CNN Path Pruning. *Lecture Notes in Computer Science (including subseries Lecture Notes in Artificial Intelligence and Lecture Notes in Bioinformatics)* 9902 LNCS, 317–325.
- Melki, I., Cardon, C., Gogin, N., Talbot, H., Najman, L., 2014. Learning-based Automatic Detection of Severe Coronary Stenoses In CT Angiographies, in: *Medical Imaging 2014: Computer-Aided Diagnosis*. volume 9035, p. 903536.
- Memari, N., Ramli, A.R., Bin Saripan, M.I., Mashohor, S., Moghbel, M., 2017. Supervised retinal vessel segmentation from color fundus images based on matched filtering and AdaBoost classifier. *Plos One* 12.
- Mo, J., Zhang, L., 2017. Multi-level deep supervised networks for retinal vessel segmentation. *International Journal of Computer Assisted Radiology and Surgery* 12, 2181–2193.
- Moccia, S., Momi, E.D., El, S., Mattos, L.S., 2018. Blood vessel segmentation algorithms – Review of methods , datasets and evaluation metrics. *Computer Methods and Programs in Biomedicine* 158, 71–91.
- Moreno, R., Smedby, Ö., 2015. Gradient-based enhancement of tubular structures in medical images. *Medical Image Analysis* 26, 19–29.
- Mou, L., Chen, L., Cheng, w.J., Gu, Z., Zhao, Y., Liu, J., 2019. Dense Dilated Network with Probability Regularized Walk for Vessel Detection. *IEEE Transactions on Medical Imaging* PP, 1–1.
- Nardelli, P., Jimenez-Carretero, D., Bermejo-Pelaez, D., Ledesma-Carbayo, M.J., Rahaghi, F.N., Estepar, R.S., 2017. Deep-learning strategy for pulmonary artery-vein classification of non-contrast ct images, in: 2017 IEEE 14th International Symposium on Biomedical Imaging, pp. 384–387.
- Nardelli, P., Jimenez-Carretero, D., Bermejo-Pelaez, D., Washko, G.R., Rahaghi, F.N., Ledesma-Carbayo, M.J., San Jose Estepar, R., 2018a. Pulmonary Artery-Vein Classification in CT Images Using Deep Learning. *IEEE Transactions on Medical Imaging* 37, 2428–2440.
- Nardelli, P., Jimenez-Carretero, D., Bermejo-Pelaez, D., Washko, G.R., Rahaghi, F.N., Ledesma-Carbayo, M.J., San Jose Estepar, R., 2018b. Pulmonary Artery-Vein Classification in CT Images Using Deep Learning. *IEEE Transactions on Medical Imaging* 37, 2428–2440.
- Nasr-Esfahani, E., Karimi, N., Jafari, M.H., Soroushmehr, S.M., Samavi, S., Nallamothu, B.K., Najarian, K., 2018. Segmentation of vessels in angiograms using convolutional neural networks, in: *Biomedical Signal Processing and Control*, Elsevier Ltd. pp. 240–251.
- Nasr-Esfahani, E., Samavi, S., Karimi, N., Soroushmehr, S.M.R., Ward, K., Jafari, M.H., Felfeliyan, B., Nallamothu, B., Najarian, K., 2016. Vessel Extraction in X-Ray Angiograms Using Deep Learning, in: *Annual International Conference of the IEEE Engineering in Medicine and Biology Society*, pp. 643–646.
- Nazir, A., Cheema, M.N., Sheng, B., Li, H., Li, P., Yang, P., Jung, Y., Qin, J., Kim, J., Feng, D.D., 2020. OFF-eNET: An Optimally Fused Fully End-to-End Network for Automatic Dense Volumetric 3D Intracranial Blood Vessels Segmentation. *IEEE Transactions on Image Processing* 29, 7192–7202.
- Ni, J., Wu, J., Wang, H., Tong, J., Chen, Z., Wong, K.K., Abbott, D., 2020. Global channel attention networks for intracranial vessel segmentation. *Computers in Biology and Medicine* 118.
- Odstrcilik, J., Kolar, R., Budai, A., Hornegger, J., Jan, J., Gazarek, J., Kubena, T., Cernosek, P., Svoboda, O., Angelopoulou, E., 2013. Retinal vessel segmentation by improved matched filtering: evaluation on a new high-resolution fundus image database. *IET Image Processing* 7, 373–383.
- Oliveira, A., Pereira, S., Silva, C.A., 2017. Augmenting Data When Training a CNN for Retinal Vessel Segmentation: How to Warp?
- Orlando, J.I., Prokofyeva, E., Blaschko, M.B., 2017. A Discriminatively Trained Fully Connected Conditional Random Field Model for Blood Vessel Segmentation in Fundus Images. *IEEE Transactions on Biomedical Engineering* 64, 16–27.
- Pohankar, N.P., Wankhade, N.R., 2016. Different methods used for extraction of blood vessels from retinal images. *IEEE WCTFTR 2016 - Proceedings of 2016 World Conference on Futuristic Trends in Research and Innovation for Social Welfare* , 1–4.
- Poletti, E., Grisan, E., 2014. A boosted optimal linear learner for retinal vessel segmentation. *Medical Imaging 2014: Computer-Aided Diagnosis* 9035, 903530.
- Rani, P., Priyadarshini, N., Rajkumar, E.R., Rajamani, K., 2016. Retinal vessel segmentation under pathological conditions using supervised machine learning.
- Rempfler, M., Schneider, M., Ielacqua, G.D., Xiao, X.H., Stock, S.R., Klohs, J., Szekely, G., Andres, B., Menze, B.H., 2014. Extracting Vascular Networks under Physiological Constraints via Integer Programming, in: *Medical Image Computing and Computer-Assisted Intervention - Miccai 2014, Pt II*. volume 8674, pp. 505–512.
- Rempfler, M., Schneider, M., Ielacqua, G.D., Xiao, X.H., Stock, S.R., Klohs, J., Szekely, G., Andres, B., Menze, B.H., 2015. Reconstructing cerebrovascular networks under local physiological constraints by integer programming. *Medical Image Analysis* 25, 86–94.
- Ricci, E., Perfetti, R., 2007. Retinal Blood Vessel Segmentation Using Line Operators and Support Vector Classification. *IEEE Transactions on Medical Imaging* 26, 1357–1365.
- Ronneberger, O., Fischer, P., Brox, T., 2015. U-net: Convolutional networks for biomedical image segmentation, in: *International Conference on Medical image computing and computer-assisted intervention*, Springer. pp. 234–241.
- Rudyanto, R.D., Kerkstra, S., van Rielwort, E.M., Fetita, C., Brillet, P.Y., Lefevre, C., Xue, W.Z., Zhu, X.J., Liang, J.M., Oksuz, I., Unay, D., Kadipaspoglu, K., Estepar, R.S., Ross, J.C., Washko, G.R., Prieto, J.C., Hoyos, M.H., Orkisz, M., Meine, H., Hullebrand, M., Stocker, C., Mir, F.L., Naranjo, V., Villanueva, E., Staring, M., Xiao, C.Y., Stoel, B.C., Fabijanska, A., Smistad, E., Elster, A.C., Lindseth, F., Foruzan, A.H., Kiros, R., Popuri, K., Cobzas, D., Jimenez-Carretero, D., Santos, A., Ledesma-Carbayo, M.J., Helmberger, M., Urschler, M., Pienn, M., Bosboom, D.G.H., Campo, A., Prokop, M., de Jong, P.A., Ortiz-de Solorzano, C., Munoz-Barrutia, A., van Ginneken, B., 2014. Comparing algorithms for automated vessel segmentation in computed tomography scans of the lung: the VESSEL12 study. *Medical Image Analysis* 18, 1217–1232.
- Saffarzadeh, V., Osareh, A., Shadgar, B., 2014. Vessel Segmentation in Retinal Images Using Multi-scale Line Operator and K-Means Clustering. *Journal of Medical Signals and Sensors* 4, 122–129.
- Samuel, D., Silveira, A., Manuel, J., Tavares, R.S., Jodas, D.S., Pereira, A.S., Tavares, J.J.M.R.J., 2017. Automatic segmentation of the lumen region in intravascular images of the coronary artery. *Medical Image Analysis* 40, 60–79.
- Sankaran, S., Schaap, M., Hunley, S.C., Min, J.K., Taylor, C.A., Grady, L., 2016. HALE: Healthy Area of Lumen Estimation for Vessel Stenosis Quantification, Springer, Cham, pp. 380–387.
- Schaap, M., Metz, C.T., van Walsum, T., van der Giessen, A.G., Weustink, A.C., Mollet, N.R., Bauer, C., Bogunović, H., Castro, C., Deng, X., Dikici, E., O'Donnell, T., Frenay, M., Friman, O., Hoyos, M.H., Kitslaar, P.H., Kriszian, K., Kühnel, C., Luengo-Oroz, M.a., Orkisz, M., Smedby, Ö., Styner, M., Szymczak, A., Tek, H., Wang, C., Warfield, S.K., Zambal, S., Zhang,

- Y., Krestin, G.P., Niessen, W.J., 2009. Standardized evaluation methodology and reference database for evaluating coronary artery centerline extraction algorithms. *Medical Image Analysis* 13, 701–714.
- Schaap, M., Van Walsum, T., Neeffjes, L., Metz, C., Capuano, E., De Bruijne, M., Niessen, W., 2011. Robust shape regression for supervised vessel segmentation and its application to coronary segmentation in cta. *IEEE Transactions on Medical Imaging* 30, 1974–1986.
- Schneider, M., Hirsch, S., Weber, B., Székely, G., Menze, B.H., Szekeley, G., Menze, B.H., 2015. Joint 3-D vessel segmentation and centerline extraction using oblique Hough forests with steerable filters. *Medical Image Analysis* 19, 220–249.
- Shen, Y., Fang, Z., Gao, Y., Xiong, N., Zhong, C., Tang, X., 2019. Coronary Arteries Segmentation Based on 3D FCN With Attention Gate and Level Set Function. *IEEE Access* 7, 42826–42835.
- Shin, S.Y., Lee, S., Yun, I.D., Lee, K.M., 2019. Deep vessel segmentation by learning graphical connectivity. *Medical Image Analysis* 58, 101556.
- Simonyan, K., Zisserman, A., 2015. Very deep convolutional networks for large-scale image recognition, pp. 1–14.
- Singh, N., Kaur, L., 2015. A survey on blood vessel segmentation methods in retinal images. 2015 International Conference on Electronic Design, Computer Networks and Automated Verification, EDCAV 2015 , 23–28.
- Sironi, A., Tekin, B., Rigamonti, R., Lepetit, V., Fua, P., 2015. Learning separable filters. *IEEE Transactions on Pattern Analysis and Machine Intelligence* 37, 94–106.
- Soomro, T.A., Afifi, A.J., Zheng, L.H., Soomro, S., Gao, J.B., Hellwich, O., Paul, M., 2019. Deep Learning Models for Retinal Blood Vessels Segmentation: A Review. *IEEE Access* 7, 71696–71717.
- Suri, J.S., Liu, K., Reden, L., Laxminarayan, S., 2002. A Review on MR Vascular Image Processing: Skeleton Versus Nonskeleton Approaches: Part II. *IEEE Transactions on Information Technology in Biomedicine* 6, 324–337.
- Tan, J.H., Acharya, U.R., Bhandary, S.V., Chua, K.C., Sivaprasad, S., 2017. Segmentation of optic disc, fovea and retinal vasculature using a single convolutional neural network. *Journal of Computational Science* 20, 70–79.
- Tetteh, G., Rempfler, M., Zimmer, C., Menze, B.H., 2017. Deep-FEXT: Deep Feature Extraction for Vessel Segmentation and Centerline Prediction, in: *Machine Learning in Medical Imaging*, volume 10541, pp. 344–352.
- Turetken, E., Benmansour, F., Andres, B., Glowacki, P., Pfister, H., Fua, P., 2016. Reconstructing Curvilinear Networks Using Path Classifiers and Integer Programming. *IEEE Transactions on Pattern Analysis and Machine Intelligence* 38, 2515–2530.
- Uslu, F., Bharath, A.A., 2019. A recursive Bayesian approach to describe retinal vasculature geometry. *Pattern Recognition* 87, 157–169.
- Vega, R., Sanchez-Ante, G., Falcon-Morales, L.E., Sossa, H., Guevara, E., 2015. Retinal vessel extraction using Lattice Neural Networks with dendritic processing. *Computers in Biology and Medicine* 58, 20–30.
- Vostatek, P., Claridge, E., Uusitalo, H., Hauta-Kasari, M., Fält, P., Lensu, L., 2017. Performance comparison of publicly available retinal blood vessel segmentation methods. *Computerized Medical Imaging and Graphics* 55, 2–12.
- Vukadinovic, D., Walsum, T.V., Manniesing, R., Rozie, S., Hameeteman, R., Weert, T.T.D., Lugt, A.V.D., Niessen, W.J., 2010. Segmentation of the Outer Vessel Wall of the Common Carotid Artery in CTA. *IEEE Transactions on Medical Imaging* 29, 65–76.
- Wang, C., Zhao, Z.Y., Ren, Q.Q., Xu, Y.T., Yu, Y., 2019. Dense U-net Based on Patch-Based Learning for Retinal Vessel Segmentation. *Entropy* 21.
- Wang, S., Yin, Y., Cao, G., Wei, B., Zheng, Y., Yang, G., 2015. Hierarchical retinal blood vessel segmentation based on feature and ensemble learning. *Neurocomputing* 149, 708–717.
- Wolterink, J.M., van Hamersvelt, R.W., Viergever, M.A., Leiner, T., Išgum, I., Hamersvelt, R.W., Viergever, M.A., Leiner, T., Išgum, I., 2019. Coronary artery centerline extraction in cardiac CT angiography using a CNN-based orientation classifier. *Medical Image Analysis* 51, 46–60.
- Wu, A., Xu, Z., Gao, M., Buty, M., Mollura, D.J., 2016. Deep vessel tracking: A generalized probabilistic approach via deep learning. *Proceedings - International Symposium on Biomedical Imaging 2016-June*, 1363–1367.
- Wu, Y.C., Xia, Y., Song, Y., Zhang, Y.N., Cai, W.D., 2018. Multiscale Network Followed Network Model for Retinal Vessel Segmentation, in: *Medical Image Computing and Computer Assisted Intervention - Miccai 2018*, Pt II, pp. 119–126.
- Xia, H.Y., Jiang, F., Deng, S.F., Xin, J., Doss, R., 2018. Mapping Functions Driven Robust Retinal Vessel Segmentation via Training Patches. *IEEE Access* 6, 61973–61982.
- Yan, Z.Q., Yang, X., Cheng, K.t.T., 2018. Joint Segment-Level and Pixel-Wise Losses for Deep Learning Based Retinal Vessel Segmentation. *IEEE Transactions on Biomedical Engineering* 65, 1912–1923.
- You, X., Peng, Q., Yuan, Y., Cheung, Y.m., Lei, J., 2011. Segmentation of retinal blood vessels using the radial projection and semi-supervised approach. *Pattern Recognition* 44, 2314–2324.
- Yu, F., Zhao, J., Gong, Y., Wang, Z., Li, Y., Yang, F., Dong, B., Li, Q., Zhang, L., 2019. Annotation-free cardiac vessel segmentation via knowledge transfer from retinal images, in: *International Conference on Medical Image Computing and Computer-Assisted Intervention*, Springer. pp. 714–722.
- Yun, J., Park, J., Yu, D., Yi, J., Lee, M., Park, H.J., Lee, J.G., Seo, J.B., Kim, N., 2019. Improvement of fully automated airway segmentation on volumetric computed tomographic images using a 2.5 dimensional convolutional neural net. *Medical Image Analysis* 51, 13–20.
- Zeng, Y.z., Zhao, Y.q., Liao, S.h., Liao, M., Chen, Y., Liu, X.y., 2018. Liver vessel segmentation based on centerline constraint and intensity model. *Biomedical Signal Processing and Control* 45, 192–201.
- Zhang, J., Chen, Y., Bekkers, E., Wang, M.L., Dashtbozorg, B., Romeny, B.M.T., 2017a. Retinal vessel delineation using a brain-inspired wavelet transform and random forest. *Pattern Recognition* 69, 107–123.
- Zhang, J., Gao, Y., Park, S.H., Zong, X., Lin, W., Shen, D., 2017b. Structured Learning for 3-D Perivascular Space Segmentation Using Vascular Features. *IEEE Transactions on Biomedical Engineering* 64, 2803–2812.
- Zhang, J., Gao, Y.Z., Park, S.H., Zong, X.P., Lin, W.L., Shen, D.G., 2016. Segmentation of Perivascular Spaces Using Vascular Features and Structured Random Forest from 7T MR Image, in: *Machine Learning in Medical Imaging*, Mlmi 2016. volume 10019, pp. 61–68.
- Zhang, L., Fisher, M., Wang, W.J., 2014. Comparative performance of texton based vascular tree segmentation in retinal images, in: *2014 IEEE International Conference on Image Processing*, pp. 952–956.
- Zhang, S., Zheng, R., Luo, Y., Wang, X., Mao, J., Roberts, C.J., Sun, M., 2019. Simultaneous Arteriole and Venule Segmentation of Dual-Modal Fundus Images Using a Multi-Task Cascade Network. *IEEE Access* 7, 57561–57573.
- Zhang, Y.S., Chung, A.C.S., 2018. Deep Supervision with Additional Labels for Retinal Vessel Segmentation Task, in: *Medical Image Computing and Computer Assisted Intervention*, pp. 83–91.
- Zhao, F., Chen, Y., Chen, F., He, X., Cao, X., Hou, Y., Yi, H., He, X., Liang, J., 2018a. Semi-Supervised Cerebrovascular Segmentation by Hierarchical Convolutional Neural Network. *IEEE Access* 6, 67841–67852.
- Zhao, F., Chen, Y., Hou, Y., He, X., 2019. Segmentation of blood vessels using rule-based and machine-learning-based methods: a review. *Multimedia Systems* 25, 109–118.
- Zhao, H., Li, H.Q., Maurer-Stroh, S., Cheng, L., 2018b. Synthesizing retinal and neuronal images with generative adversarial nets. *Medical Image Analysis* 49, 14–26.
- Zhao, M.L., Miles, B., Hamarneh, G., 2017. Leveraging Tree Statistics for Extracting Anatomical Trees from 3D Medical Images.
- Zheng, Y., John, M., Liao, R., Nöttling, A., Boese, J., Kempfert, J., Walther, T., Brockmann, G., Comaniciu, D., 2012. Automatic aorta segmentation and valve landmark detection in C-Arm CT for transcatheter aortic valve implantation. *IEEE Transactions on Medical Imaging* 31, 2307–2321.
- Zheng, Y., Loziczonek, M., Georgescu, B., Zhou, S.K., 2011. Machine Learning Based Vesselness Measurement for Coronary Artery Segmentation in Cardiac CT Volumes, in: *Spie*.
- Zhou, J.H., Chang, S., Metaxas, D., Axel, L., 2007. Vascular structure segmentation and bifurcation detection, in: *2007 4th IEEE International Symposium on Biomedical Imaging : Macro to Nano*, Vols 1-3, pp. 872–+.
- Zreik, M., van Hamersvelt, R.W., Wolterink, J.M., Leiner, T., Viergever, M.A., Išgum, I., van Hamersvelt, R.W., Leiner, T., Viergever, M.A., Wolterink, J.M., Leiner, T., Viergever, M.A., Išgum, I., 2018. A Recurrent CNN for Automatic Detection and Classification of Coronary Artery Plaque and Stenosis in Coronary CT Angiography. *IEEE Transactions on Medical Imaging* 38, 1588–1598.